

Review

Electrochemical Synthesis of Functional Coatings and Nanomaterials in Molten Salts and Their Application

Yuriy Stulov , Vladimir Dolmatov , Anton Dubrovskiy and Sergey Kuznetsov *

Tananaev Institute of Chemistry of the Federal Research Centre “Kola Science Centre of the Russian Academy of Sciences”, 184209 Apatity, Russia

* Correspondence: s.kuznetsov@ksc.ru

Abstract: Nanomaterials are widely used in modern technologies due to their unique properties. Developing methods for their production is one of the most important scientific problems. In this review, the advantages of electrochemical methods for synthesis in molten salts of nanostructured coatings and nanomaterials for different applications were discussed. It was determined that the nanostructured Mo₂C coatings on a molybdenum substrate obtained by galvanostatic electrolysis have a superior catalytic activity for the water-gas shift reaction. The corrosion-resistant and wear-resistant coatings of refractory metal carbides on steels were synthesized by the method of currentless transfer. This method also was used for the production of composite carbon fiber/refractory metal carbide materials, which are efficient electrocatalysts for the decomposition of hydrogen peroxide. The possibility to synthesize GdB₆ nanorods and Si and TaO nanoneedles by potentiostatic electrolysis was shown.

Keywords: electrochemical synthesis; molten salts; nanostructured coatings; refractory carbide coatings; carbon fibers; nanorods; nanoneedles



Citation: Stulov, Y.; Dolmatov, V.; Dubrovskiy, A.; Kuznetsov, S. Electrochemical Synthesis of Functional Coatings and Nanomaterials in Molten Salts and Their Application. *Coatings* **2023**, *13*, 352. <https://doi.org/10.3390/coatings13020352>

Academic Editor: JongHyeon Lee

Received: 2 December 2022

Revised: 27 January 2023

Accepted: 30 January 2023

Published: 3 February 2023



Copyright: © 2023 by the authors. Licensee MDPI, Basel, Switzerland. This article is an open access article distributed under the terms and conditions of the Creative Commons Attribution (CC BY) license (<https://creativecommons.org/licenses/by/4.0/>).

1. Introduction

In recent years, nanostructured and nanoscale materials have been of great interest because of the unique mechanical, electrical, optical, and chemical properties possessed by such materials due to the small size of their components (e.g., grains, phase inclusions, layers, pores, etc.). The possibility of obtaining nanomaterials with a given structure provides a wide range of opportunities for the creation of new functional materials with unique sets of characteristics [1]. Nanomaterials are of great applied importance for solving problems of energy storage and conversion energy [2–4]; they are also used as catalysts [5–8], electrocatalysts [9], protective coatings and structural materials [10,11].

To the present day, a great number of different methods and approaches have been developed for the synthesis of nanomaterials [12–15]. According to [15] they can be divided into three groups: biological, physical, and chemical. In the current study, we will not describe all methods of nanomaterials synthesis in detail, but we will focus on some of the most common ones, including sol-gel [16–20], micellar [21–23], hydrothermal [24–27], vapor deposition [28–32], ultrasonic [33–37], microwave [38–41], and electrochemical [42–50].

Electrochemical methods of synthesizing nanomaterials and functional materials have a number of advantages over other methods [51]. For example:

- electrolysis of melts using pulsed and reversible currents provides the ability to easily adjust the structure, thickness, porosity, roughness, grain size and texture of electroplated coatings and materials;
- a large number of environments for synthesis (both aqueous and non-aqueous) used for various purposes;
- electrodeposition parameters determined at a laboratory scale can be transferred to the industrial scale;

- high purity of the obtained coatings and materials even if low-quality initial reagents are used, since metals are refined in the process of electrolysis;
- low operating costs and low costs of electrochemical equipment.

On the other hand, the use of molten salts such as chlorides and fluorides of alkali metals as a medium in the electrochemical synthesis of nanomaterials makes it possible to increase the current density due to a high electric conductivity and thereby to intensify the synthesis processes. Electrochemical synthesis in molten salts leads to the appearance of strong electric and magnetic fields in the near-electrode layer (the electric field strength near the cathode is 10^9 – 10^{10} V m⁻¹ [52]). Therefore, the synthesis can proceed under conditions far from the thermodynamical equilibrium, which significantly expands the number of obtained compounds and their phase modifications as compared to other methods of nanomaterial production.

A large number of studies are devoted to obtaining silicon-based nanomaterials in various molten salts using electrochemical methods [53–61]. For example, methods of producing silicon-based nanomaterials for utilization in advanced power engineering are reviewed in [55,57,59–61]. By varying the electrolyte composition, electrolysis parameters and process temperature, it becomes possible to synthesize nanowires and nanotubes.

The synthesis of carbon-based nanomaterials in molten salts has been the subject of many reviews and articles. In review [62], the methods and mechanisms of synthesis of nanomaterials based on graphene and its oxide in various melts are discussed in detail. Reducing the amount of carbon dioxide emissions in the atmosphere has become an urgent problem, and the electroreduction of CO₂ in molten salts can contribute to solving this challenge. In works [63–73], the processes and mechanisms of electroreduction of carbon dioxide in various melts leading to the production of various carbon nanoparticles have been investigated. One study [64] reveals the effect of the electrolysis temperature in molten Li-Na-K carbonates on the shape of carbon nanomaterials. At a process temperature below 850 K, carbon nanosheets are formed on the cathode, and nanotubes are formed at a higher temperature. In the paper [65], the principle possibility of carbon nanotube generation by the electrolysis of molten salts saturated by carbon dioxide was shown. Kushkov et al. [68] found that, depending on the experimental conditions, the electrolysis of molten alkali metal carbonates led to the synthesis of carbon nanotubes or fullerenes C₆₀ or C₇₀. Electrochemical methods to synthesize carbon nanotubes and various carbon nanostructures from CO₂ in molten CaCl₂-NaCl-CaO were discussed in [72].

For the nanotechnology of carbon materials, it is of great interest to produce nanodiamonds in molten salts. It was shown in [74] that single Li₂CO₃ nanocrystals (<30 nm) can be synthesized by the injection of moist CO₂ into molten LiCl containing Li₂O. The subsequent cathodic polarization of a graphite rod immersed in the molten salt led to the formation of carbon-encapsulated lithium carbonate nanoparticles. Upon heating in ambient-pressure air, these nanostructures acted as high-pressure nanocrucibles, creating diamond crystallites within lithium carbonate.

The electrochemical methods allow to synthesize carbides of different metals, which can be used for surface protection against oxidation or corrosion and as catalysts or electrocatalysts. In studies [75,76] voltammetric investigations of tungsten and carbon-containing melts were carried out to find the conditions for a high-temperature electrochemical synthesis of nanostructured tungsten carbide coatings and nanopowders. Binary tungsten-molybdenum carbide nanopowders were fabricated by high-temperature electrochemical synthesis from tungstate-molybdate-carbonate melts [77].

Analysis of available literature data shows that electrochemical synthesis in molten salts is a promising method for obtaining coatings and nanomaterials.

Of course, this article is not a complete review of all the data available in the literature on the production of coatings and nanomaterials in molten salts. The aim of the present work was to introduce our results on electrochemical synthesis in molten salts of nanostructured coatings and nanomaterials used for different applications.

2. Materials and Methods

In this work, we used chloride-fluoride electrolytes for the synthesis of nanostructured coatings and nanomaterials.

Sodium and potassium chlorides (Prolabo 99.5% min) were recrystallized in distilled water to remove various insoluble impurities. Afterwards they were calcined in a muffle furnace at 773 K. Then, NaCl and KCl were mixed (with a molar ratio of 1:1) and evacuated to a residual pressure of 0.6 Pa at 298, 473, 673, and 823 K; following that, the NaCl and KCl mixture was melted in a purified and dried argon atmosphere.

Sodium fluoride (Prolabo 99.5% min) was refined from impurities using the method of directional crystallization, which is described elsewhere [78].

Li_2CO_3 (Sigma-Aldrich, St. Louis, MI, USA, 99% min) and $\text{Na}_2\text{MoO}_4 \cdot \text{H}_2\text{O}$ (Sigma-Aldrich, 99.5% min) were dehydrated for 24 h at 473 K. Chromium trichloride (Sigma-Aldrich, anhydrous, 99.99% min) was used without additional treatment.

Potassium heptafluoronioate, heptafluorotantalate, and hexafluorosilicate were synthesized at the experimental facility of the Tananaev Institute of Chemistry-Subdivision of the Federal Research Centre, at the Kola Science Centre of the Russian Academy of Sciences. The content of metallic impurities in the synthesized salts did not exceed 10^{-3} wt.% according to mass spectroscopy data. The purification methods of K_2NbF_7 , K_2TaF_7 , and K_2SiF_6 are described in literature [79–81].

Potassium tetrafluoroborate (Sigma-Aldrich, 99.99% min) was used without additional treatment. GdF_3 was synthesized by heating a mixture of Gd_2O_3 and $[\text{NH}_4][\text{HF}_2]$ in an argon atmosphere [78]. The procedures for obtaining K_3TaOF_6 and CsCl were described in details elsewhere [82].

A detailed description of the experimental setup, instruments and materials used for synthesis, identification and investigation of the morphology, and properties of the synthesized coatings and nanomaterials are given in [83–85].

Other specific techniques are described in the sections below.

3. Results and Discussions

3.1. Nanostructured Catalytic Coatings Mo_2C

One of the promising areas of hydrogen energy is the direct placement of an integrated device on board a vehicle, which includes a fuel processor in combination with a fuel cell. As a result of the transformation of gasoline or natural gas, hydrogen is obtained, which contains about 12 vol % CO. The carbon monoxide steam reforming reaction (SRR) is used to remove carbon monoxide from the hydrogen-rich gas, since CO is a catalytic poison to the proton exchange membrane of the fuel cell. The high-temperature steam reforming reaction is usually carried out on ferrochrome ($\text{Fe}_3\text{O}_4/\text{Cr}_2\text{O}_3$) as a catalyst at temperatures of 573–723 K, which makes it possible to reduce the CO content to 2 vol % and obtain an additional amount of hydrogen. This product is then subjected to a low-temperature steam reforming reaction using a $\text{Cu}/\text{ZnO}/\text{Al}_2\text{O}_3$ catalyst at a temperature range of 433–523 K, which reduces the CO concentration to 0.1% by volume. However, the low-temperature catalyst occupies approximately 70% of the volume of the entire fuel processor catalytic system and is also pyrophoric due to the oxidation of Cu to Cu_2O or CuO, making it potentially hazardous. Strict temperature control is necessary to carry out a low-temperature SRR, which makes the $\text{Cu}/\text{ZnO}/\text{Al}_2\text{O}_3$ catalyst impractical.

Thus, the search for a catalyst with high activity at 473–523 K, capable of reducing the CO concentration to 0.1 vol % for use in automobiles and other vehicles, remains relevant. A new class of catalytic systems based on refractory metal carbides can be used for the carbon monoxide steam reforming reaction.

3.1.1. Electrochemical Synthesis

Based on the analysis of the peculiarities of molybdenum and carbon electrodeposition, an NaCl-KCl-Li₂CO₃-Na₂MoO₄ chloride-carbonate-molybdate melt was chosen for electrochemical synthesis. As the substrate, molybdenum plates (99.99 wt.% Mo), 40 mm long, 10 mm wide, and 0.1 mm thick were used. Electrochemical synthesis of Mo₂C coatings was carried out at the following conditions: temperature 1123 K, cathodic current density 5 mA cm⁻², time of electrolysis 7 h, and the glassy carbon (SU-2000) ampoule was used as the anode. X-ray phase and microstructural analyses, scanning electron microscopy, and the BET method were used to characterize the obtained coatings.

It is important that the obtained coatings are β-Mo₂C monophase semi-carbide with a hexagonal crystalline lattice (Figure 1). At the same time, bulk Mo₂C contains at least several weight percent of cubic molybdenum carbide, which significantly reduces its catalytic activity and stability in the carbon monoxide steam reforming reaction. The formation of hexagonal Mo₂C during electrochemical synthesis is the result of specific electrocrystallization conditions (electric field, double layer, and high temperature) [52].

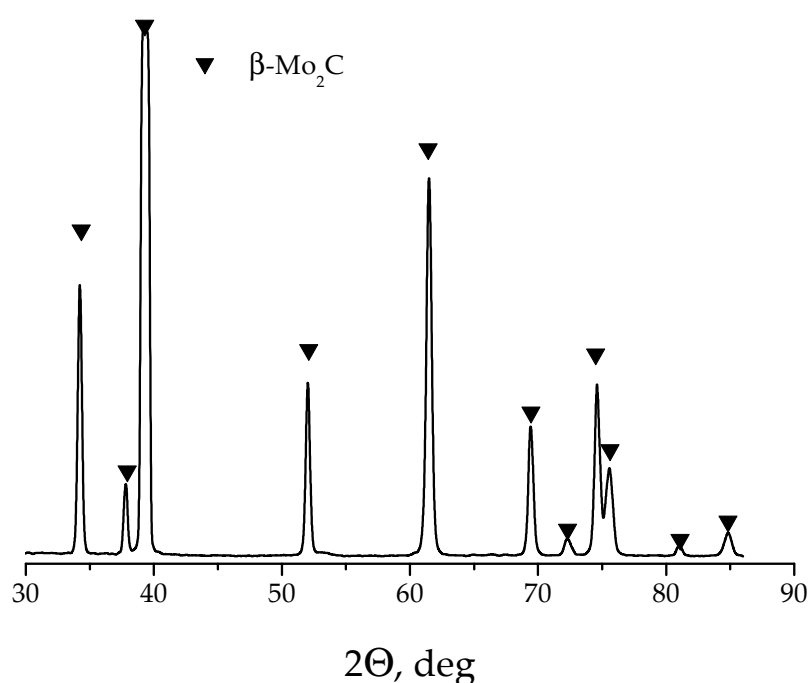


Figure 1. X-ray powder diffraction patterns of the molybdenum carbide coating on molybdenum substrates obtained at 1123 K and a current density of 5 mA cm⁻² from the NaCl-KCl-Li₂CO₃ (1.5 wt.%)-Na₂MoO₄ (8.0 wt.%) melt (solid line), data points indicate the reference sample.

Joint electroreduction of MoO₄²⁻ and CO₃²⁻ ions resulted in the formation of 50 μm thick Mo₂C coatings and can be in general described by the reaction:



The morphology of the Mo₂C coating is presented in Figure 2. The figure shows that the obtained coating is nanostructured, and consists of a large number of pores with sizes ranging from 300 nm to 3 μm and Mo₂C nanoneedles.

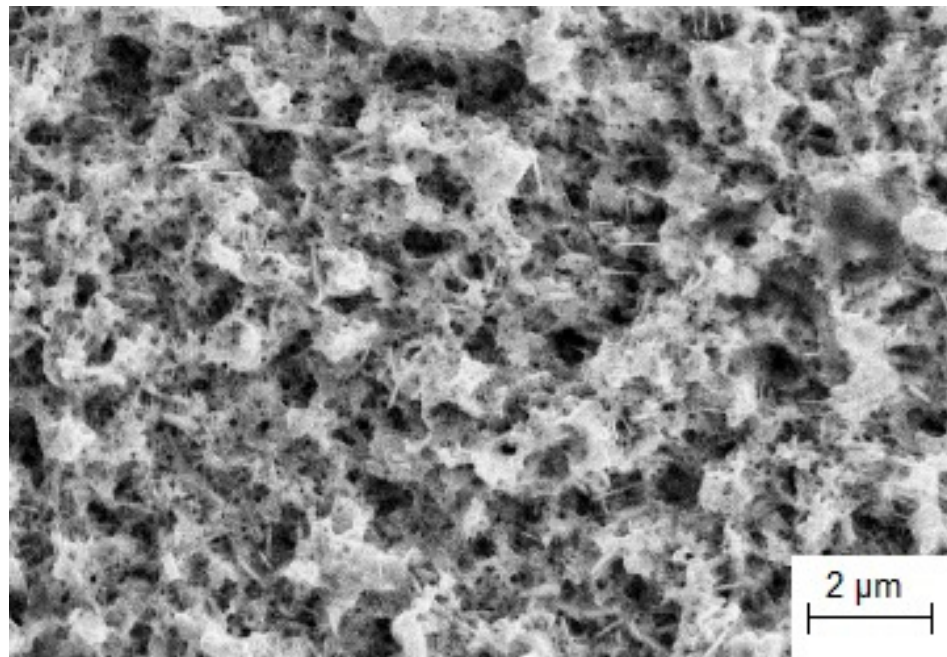


Figure 2. Morphology of molybdenum carbide coating on a molybdenum substrate. $T = 1123$ K, $i = 5$ mA cm⁻², melt-NaCl-KCl-Li₂CO₃ (1.5 wt.%)–Na₂MoO₄ (8.0 wt.%).

3.1.2. Catalytic Activity

The steady-state steam reforming reaction rate for the Mo₂C/Mo composition was three orders of magnitude higher than for the Mo₂C bulk phase and the commercial Cu/ZnO/Al₂O₃ catalyst (Figure 3).

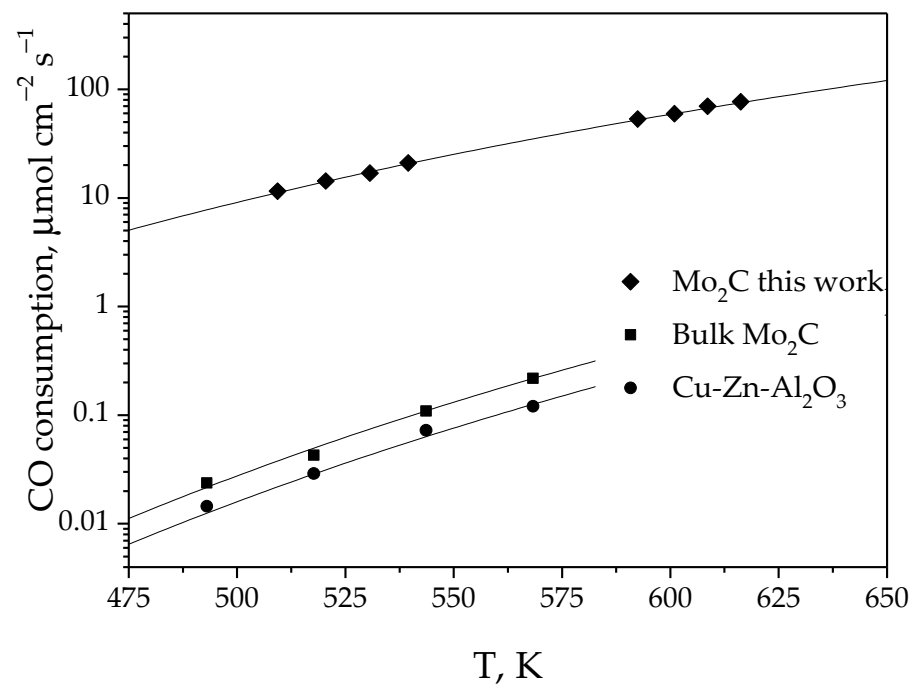


Figure 3. Temperature dependence of the steam reforming reaction rate over different catalysts. Reaction conditions: $p_{CO} = 300$ Pa, $p_{H_2O} = 760$ Pa, $p_{CO_2} = 1.2$ kPa, $p_{H_2} = 40$ kPa and balanced helium. The gas flow rate is 50 cm³ min⁻¹ (STP).

The specific surface area (BET surface) of the Mo₂C coating was 38 m² g⁻¹. The BET surface of bulk Mo₂C was much higher (61 m² g⁻¹) [86]. Despite this, the catalytic activity of the bulk Mo₂C was much lower than that of the catalysts obtained by electrolysis. This can be explained by the presence of cubic modification in the bulk Mo₂C composition, which significantly reduces the SRR rate.

Methane formation was not observed throughout the entire temperature range in which the Mo₂C/Mo coatings were tested. The catalytic activity remained constant over 5000 h of testing. The coatings also remained stable during cyclic temperature tests, while the activity of industrial catalysts decreased.

Thus, by electrochemical synthesis in molten salts, we obtained a new Mo₂C/Mo-based catalytic system for a low-temperature steam reforming reaction. The catalytic activity of the composition, obtained by simultaneous reduction of electroactive MoO₄²⁻ and CO₃²⁻ particles, was three orders of magnitude higher than that of the bulk Mo₂C and commercially available Cu-ZnO-Al₂O₃ catalyst.

3.2. Wear and Corrosion Resistance Coatings on Steels

The main requirements for hard alloys as cutting, milling, and drilling tools are wear resistance, chemical stability at high temperatures, and superior mechanical properties. Current research shows that the local temperature on the surface of these tools increases greatly during tool usage, resulting in oxidation, changes in composition, and surface degradation over time. In addition, these materials sometimes operate in aggressive environments. The corrosion rate of materials is significantly affected by the pH of the environment. Materials based on the refractory metal carbides show a good resistance in acidic electrolytes [87].

The modification of a tool's surface with films and coatings of different compositions can be carried out by many methods. These coatings determine the surface properties [88,89]. Currently NbC and TaC, with the addition of WC, are effectively used as cutting tools [90]. Tantalum carbide is used in the engine and aerospace industries due to its resistance to high-temperature oxidation [91].

Various techniques of obtaining chromium carbide coatings, such as chemical vapor deposition [92], metallothermic reduction of Cr₂O₃/C mixtures [93], and magnetron sputtering [94] were reviewed in [92–96]. It is shown that the deposition of Cr₂C₃ as a coating on steel leads to an increase in the hardness and wear resistance and reduces the friction coefficient [93,94].

In [97], different methods of synthesis of protecting coatings are discussed. It was concluded [97] that coating deposition by molten salt electrolysis is a prospective way for obtaining smooth and uniform coatings on complex-shape samples.

Previously, we have thoroughly studied [98] the processes of alloy formation during electrodeposition of chromium on the surface of steels with the formation of chromium carbide coatings of different compositions.

3.2.1. Currentless Transfer: A Simple Way to Obtain Refractory Carbide Coatings

An alternative method for synthesizing coatings of refractory metal carbides on steels is currentless transfer (CT) [99]. It is important to note that CT is an electrochemical method, and synthesis by CT is subject to the laws of electrochemical thermodynamics, kinetics, and reaction diffusion in solids [98,100–102].

A schematic diagram of CT in molten salts is shown in Figure 4. During the process, metal-salt reactions occur and metal cations with an intermediate oxidation state are formed disproportionately on the surface of steel (or another carbon-containing material) to form a refractory metal carbide and a cation in a higher oxidation state. The driving force of the CT is the Gibbs (ΔG_r) energy of the carbide-forming reaction. The carbide with the smallest (more negative) value of ΔG_r will be formed [99].

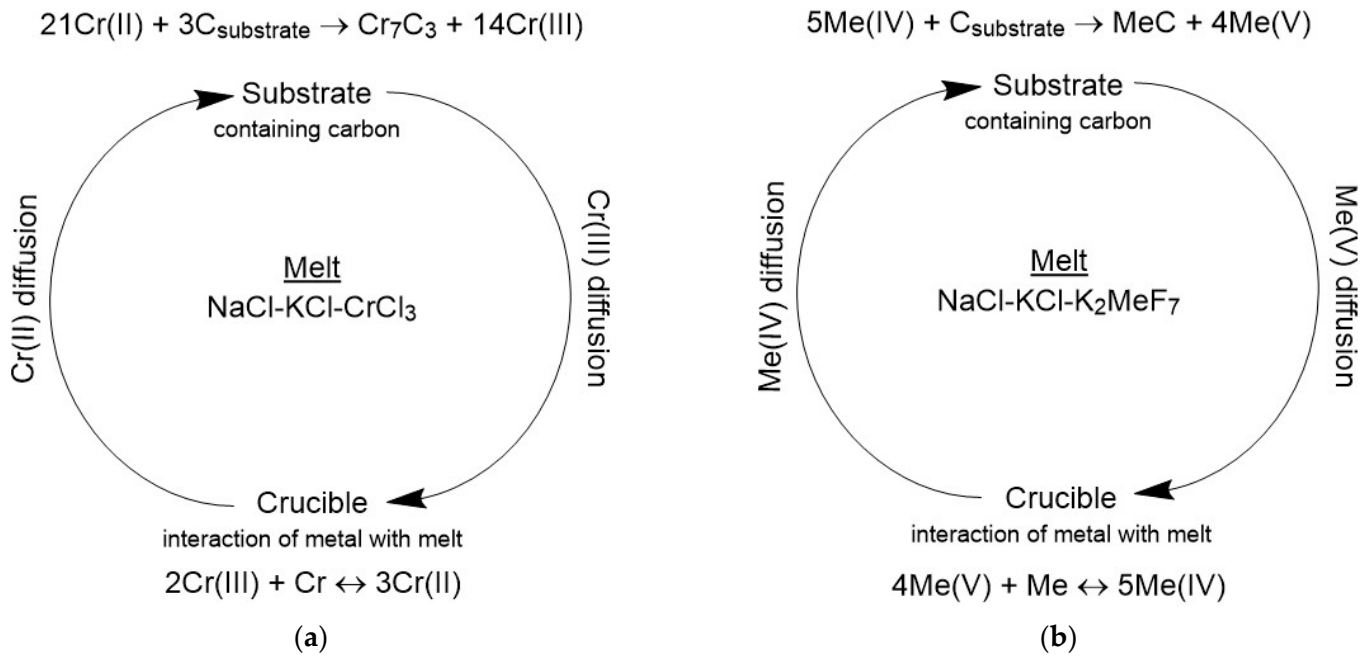


Figure 4. Principle scheme of coating synthesis by the CT in molten salts. (a)— Cr_7C_3 chromium carbide; (b)— MeC carbides ($\text{Me} = \text{Nb}, \text{Ta}$).

Figure 5 shows the temperature dependencies of the Gibbs energy per 1 mole of the product for the formation of chromium, tantalum, and niobium carbides from the elements. It was shown that the formation of Cr_7C_3 , TaC , and NbC carbides is the most preferable. It also follows from the thermodynamic data that the synthesis of chromium carbides on steels is preferable at higher temperatures, as evidenced by the decrease in ΔG_r with increasing temperature. For niobium and tantalum carbides the temperature dependence of ΔG_r is different, and ΔG_r increases (becomes less negative) with increasing temperature. However, with increasing temperature the melt viscosity decreases, and diffusion fluxes of metal complexes in various degrees of oxidation through the electrolyte increase. This leads to the intensification of NbC and TaC formation on steels with increasing temperature despite being less thermodynamically favorable.

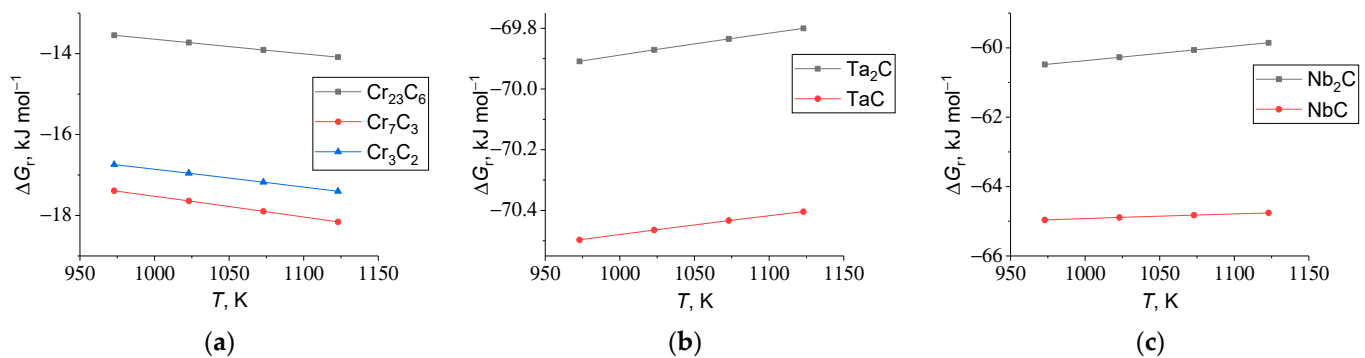


Figure 5. Temperature dependencies of the Gibbs energy for the formation reactions of (a)—chromium, (b)—tantalum, and (c)—niobium carbides from the elements.

Based on these considerations, the optimal conditions for the synthesis of carbide coatings by the CT method were selected. An equimolar NaCl-KCl mixture was used as an electrolyte, the process temperature was 1173 K, the concentrations of refractory metal salts (CrCl_3 , K_2TaF_7 and K_2NbF_7) were 30 wt.%, and the synthesis time varied from 3 up to 24 h [103].

The obtained coatings were analyzed by XRD, which showed the formation of Cr_7C_3 , TaC and NbC coatings (Figure 6), in perfect agreement with the thermodynamic data. The peaks of diffraction patterns corresponding to the substrate are caused by the insignificant thickness of the synthesized coatings.

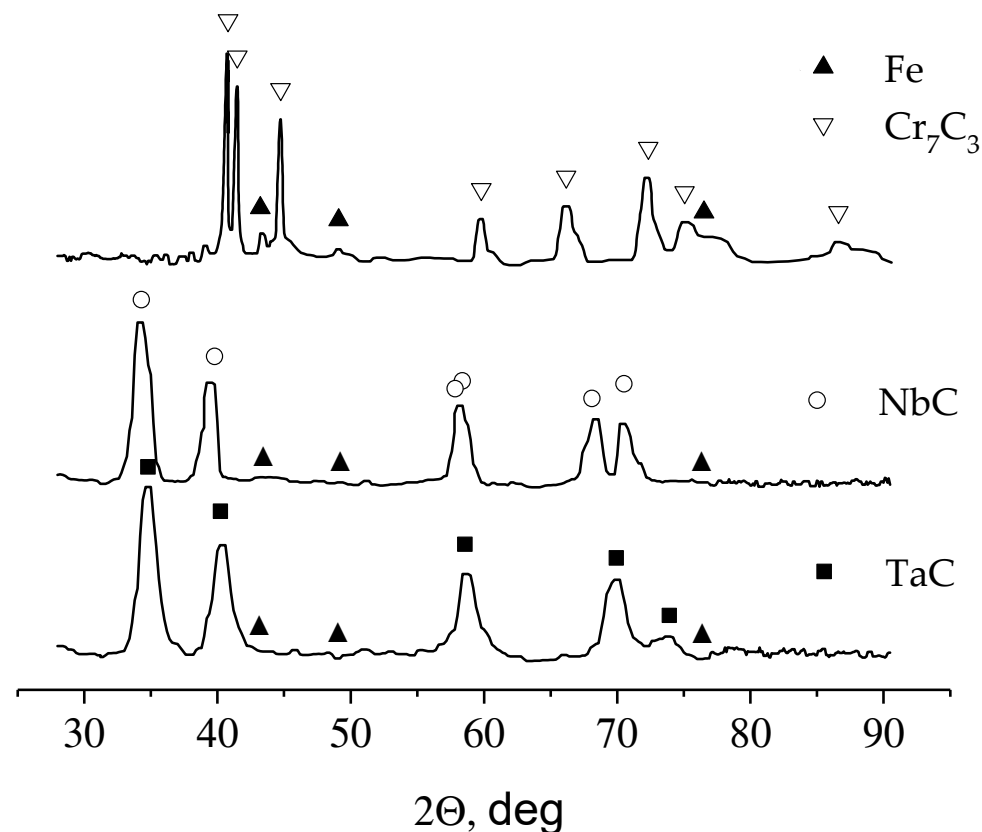


Figure 6. XRD patterns of the refractory carbide coatings on the St3 steel substrate (solid line), data points indicate the reference samples.

3.2.2. Protective Properties of Refractory Carbide Coatings

Cross-section was used to determine the thickness of synthesized refractory metal carbide coatings. In general, the thickness of the coatings obtained by the CT method depends on the duration of the process, the diffusion rate, and the carbon content in the substrate. In our case, the coating thicknesses were 1–2 microns. The morphologies of niobium carbide coatings formed at various synthesis durations on St.3 steel are presented in Figure 7. The coatings were composed of densely packed spherical particles with a diameter of 1–2 μm . If the synthesis time was 3 h (Figure 7a), the coating was not continuous. To obtain continuous coatings, the synthesis time was increased to 8 h (Figure 7b).

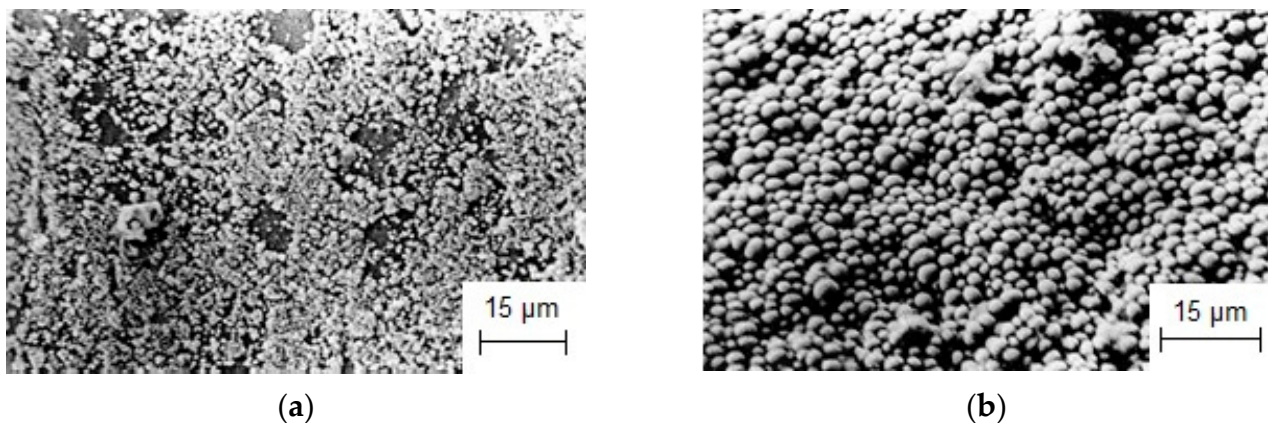


Figure 7. St.3 substrate surface morphology after its (a)—3 h exposure and (b)—8 h exposure in the NaCl-KCl-K₂NbF₇ (30 wt.%)—Nb melt at 1173 K.

Samples coated with Cr₇C₃, NbC and TaC were tested for corrosion resistance in concentrated mineral acids and for wear resistance by the following methods. The corrosion rate was determined by a gravimetric method using cylindrical samples with a length of 30 mm and a diameter of 7 mm. After deposition of the coatings and electrolyte removal, the samples were degreased with refined ethyl alcohol. The corrosion rate was determined at 298 K for 48 h as a mass loss of the sample through a surface area unit per unit of time. At the end of the sample exposure in concentrated mineral acids, corrosion products were removed mechanically, the samples were degreased again, and were weighed on analytical scales with an accuracy of up to 1×10^{-5} g.

The wear rate was measured as the weight loss of the coated sample relative to the original sample, on the SMTs-2 friction machine (LLC “Precision Instruments”, Ivanovo, Russia) at a specific load of 5 mPa, in transformer oil, at a slip velocity of 1.2 m s^{-1} , and on a path segment of 2000 m.

The results of the corrosion and wear resistance tests are shown in Figure 8. Refractory metal carbide coatings substantially reduced the corrosion rate of steel samples in concentrated acids, especially for H₂SO₄ and HCl (Figure 8a). Of course, the quality of obtained coatings (porosity) affects the results to a certain degree. Due to high hardness values of refractory metal carbides and their good adhesion with the substrate, the loss of mass as a result of mechanical wear is reduced by 3–5 times compared with the reference sample (Figure 8b).

Our studies showed that to achieve a good corrosion resistance of samples with Cr₇C₃, NbC and TaC coatings, the required thickness of protective coatings should be 1–3 μm. At the same time, thin films with a thickness of 100–700 nm obtained at a shorter duration of synthesis are sufficient only to impart resistance to mechanical wear.

The combination of high corrosion and wear resistance makes the investigated coatings a promising material for aggressive media with abrasive wear. These coatings have been tested in industrial facilities. Deposition of niobium carbide coatings on parts of crude oil pumps improved their lifetime by 3–4 times (tested by LLC “New technology”, Russia, Nefteyugansk). Tests carried out by LLC “Ecotech” (Russia, Apatity) showed that the coatings of Cr₇C₃ or TaC on the rubber-cutting knives made of St3 can increase their wear resistance and increase a tool service life by a factor of 2.0 (Cr₇C₃) and 2.5 (TaC).

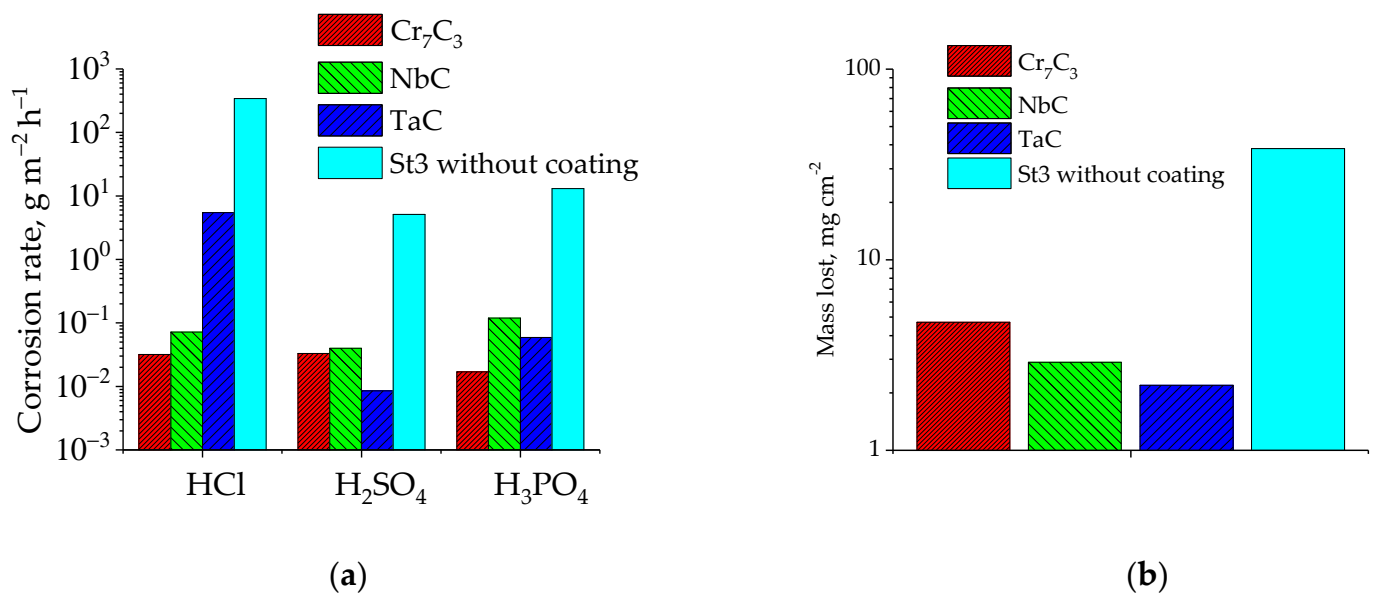


Figure 8. (a)—Corrosion rates of steel/refractory metal carbide coatings in concentrated mineral acids and (b)—mass loss due to mechanical wear.

3.3. Electrocatalytic Compositions Carbon Fiber/Refractory Metal Carbide

The application of cheap refractory metal carbides as catalysts and electrocatalysts instead of expensive noble metals is preferable for some oxidation or reduction processes [104]. Carbon fibers can serve as a substrate for the electrochemical deposition of coatings and crystals of refractory metal carbides from molten salt media. Obtaining refractory metal carbide-carbon fiber composites using such processes is operationally quite simple and not energy consuming.

Conducting electrocatalytic reactions instead of traditionally catalytic ones has a number of advantages. For example, it is possible to control the reaction kinetics by adjusting the potential, which directly affects the activation energy of the conducted process [105], as well as the environmental friendliness of electrocatalysis since an electron is involved in the reaction as an oxidizing or reducing agent, and there are no hazardous reaction by-products [105,106].

3.3.1. Synthesis of Refractory Metal Carbide Coatings on Carbon Fibers

The synthesis of transition metal carbide/carbon fiber composites was carried out by the CT method described above (Section 3.2.1). X-ray diffraction patterns of all synthesized composites are presented in Figure 9. According to XRD analysis, tantalum carbide had a cubic structure with a border-centered crystal lattice, niobium carbide had a cubic crystal lattice, and crystals of the Mo_2C phase had a hexagonal structure.

Figure 10 shows micrographs of carbon fibers coated with tantalum carbide (a) and a cross-section of a single fiber (b). The micrographs show that the fibers were not spliced together, and the coatings were uniform both in the cross-section and along the fiber.

Carbon fibers with niobium carbide coatings are shown in Figure 11. The diameter of the carbon fibers was approximately $7 \pm 1 \mu\text{m}$. The thickness of the tantalum and niobium carbide coatings on the carbon fiber was from a few tens of nanometers to a couple hundred nanometers. No other compound phases were detected between the carbon fiber and the coating.

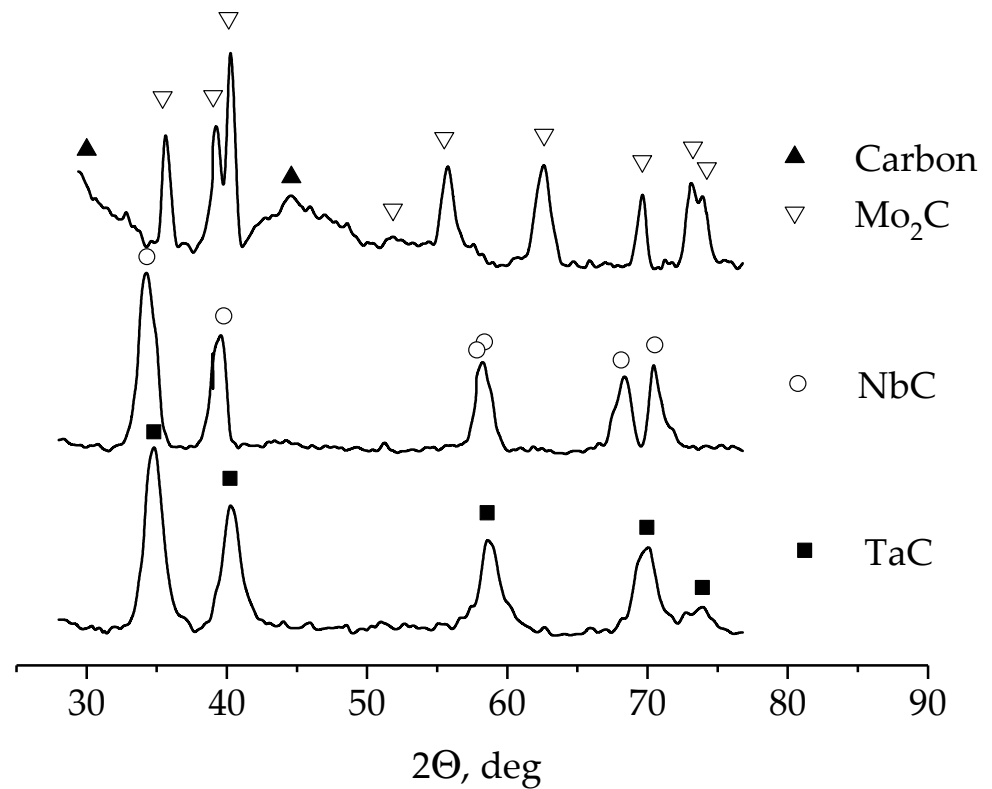


Figure 9. X-ray diffraction patterns of TaC, NbC coatings and Mo_2C crystals obtained by electrochemical methods in molten salts on the surface of carbon fibers (solid line). Data points indicate the reference samples.

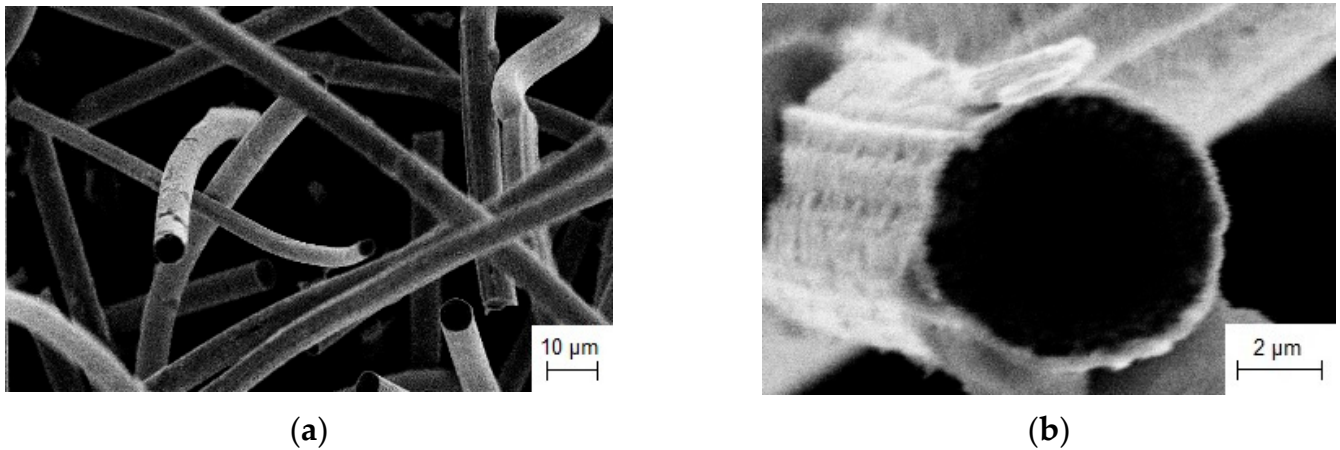


Figure 10. Micrographs of the tantalum carbide-carbon fiber composite at different scale. (a)—Overall view and (b)—cross-section of a single fiber. Synthesis conditions: CT in $\text{NaCl-KCl-K}_2\text{TaF}_7$ (30 wt.%)–Ta melt at 1123 K for 24 h.

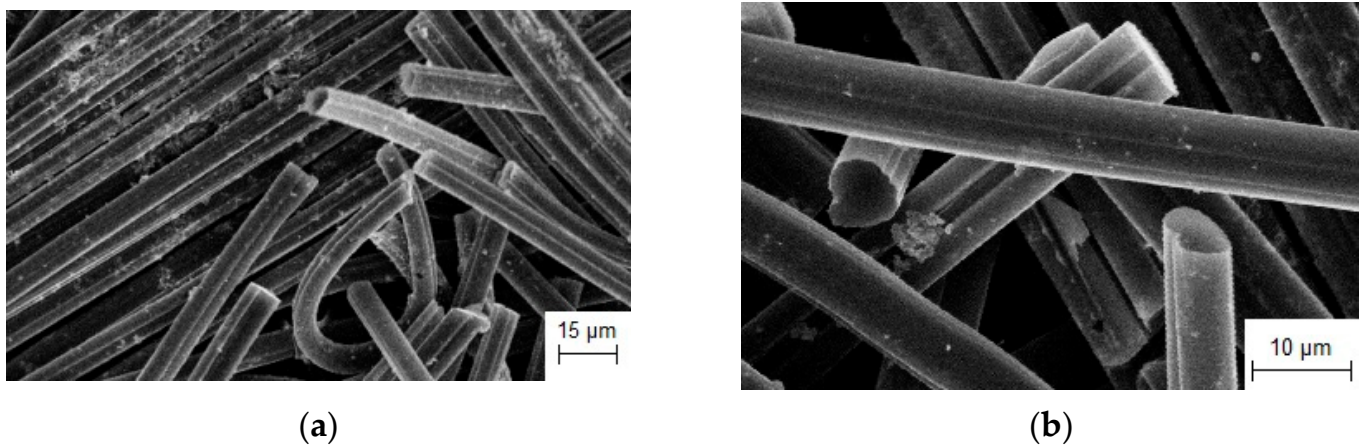


Figure 11. Micrographs of the niobium carbide-carbon fiber composite at different scale. (a)—Overall view and (b)—cross-sections of fibers. Synthesis conditions: CT in NaCl-KCl-K₂NbF₇ (30 wt.%)–Nb melt at 1123 K for 24 h.

The Mo₂C phase was also obtained on carbon fibers by CT in molten salts. The melt in this case contained sodium molybdate, Na₂MoO₄. It was found that increasing the exposure time of the carbon fiber in the melt leads to an increase in the amount of Mo₂C crystals. The Mo₂C crystals had a well-defined structure with a crystal size of ~7–21 μm (Figure 12).

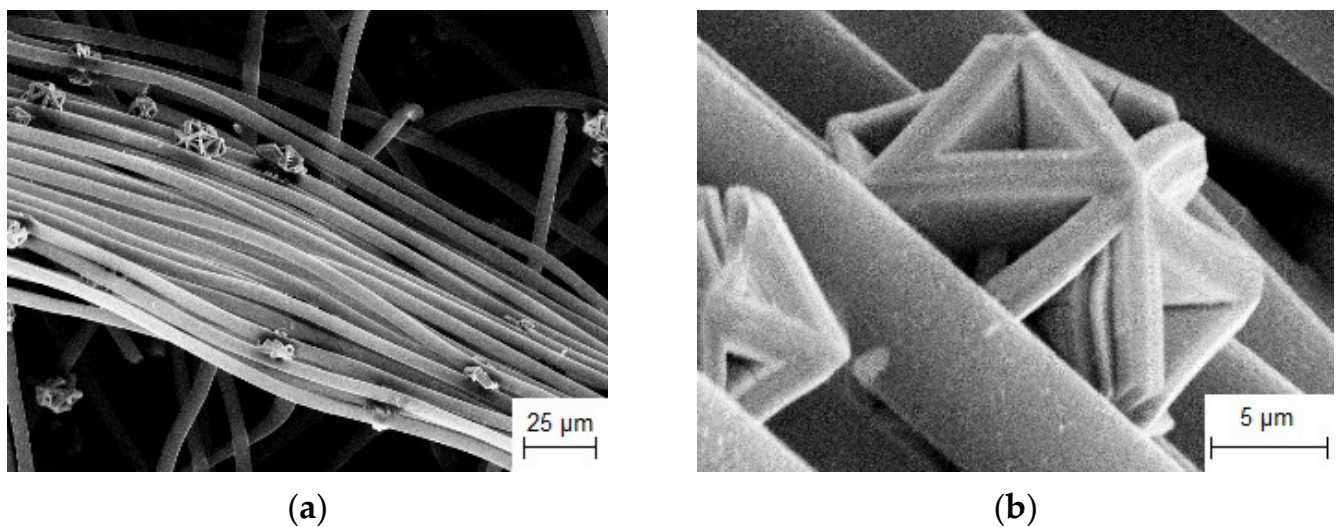


Figure 12. Micrographs of the molybdenum carbide-carbon fiber composite at different scale. (a)—Overall view and (b)—a single Mo₂C crystal. Synthesis conditions: CT in NaCl-KCl-Na₂MoO₄ (15 wt.%)–Mo melt at 1123 K and for 1 h.

3.3.2. Investigation of the Electrocatalytic Activity of Composites Based on Refractory Metal Carbide on Carbon Fiber

The kinetics of electrocatalytic decomposition of hydrogen peroxide on the surface of refractory metal carbides (TaC, NbC, Mo₂C) can be investigated by measuring the volume of evolved gases per unit of time. Decomposition of hydrogen peroxide proceeds with the emission of gaseous products: oxygen is emitted at the anode, which was the studied composite material, and hydrogen is emitted at the cathode, which was an uncoated carbon fiber.

To compare the results of studying the kinetics of the hydrogen peroxide decomposition reaction on refractory metal carbide-carbon fiber composites with the kinetics of the same reaction using traditional catalysts as copper and platinum, we used 5 mm² metal electrodes. However, it is difficult to estimate the surface area of electrodes made of composites of refractory metal carbides. Their specific surface area is 5–15 m² g⁻¹. In all our experiments, the same linear dimensions of the composite electrodes were used, and the same immersion depth in hydrogen peroxide solution was maintained.

The graphical analysis of the kinetic dependences (Figure 13) established the zero order of the electrocatalytic reaction of hydrogen peroxide decomposition [107]. It can be described by the kinetic equation of the form $v = k$, where v is the reaction rate, and k is the reaction rate constant.

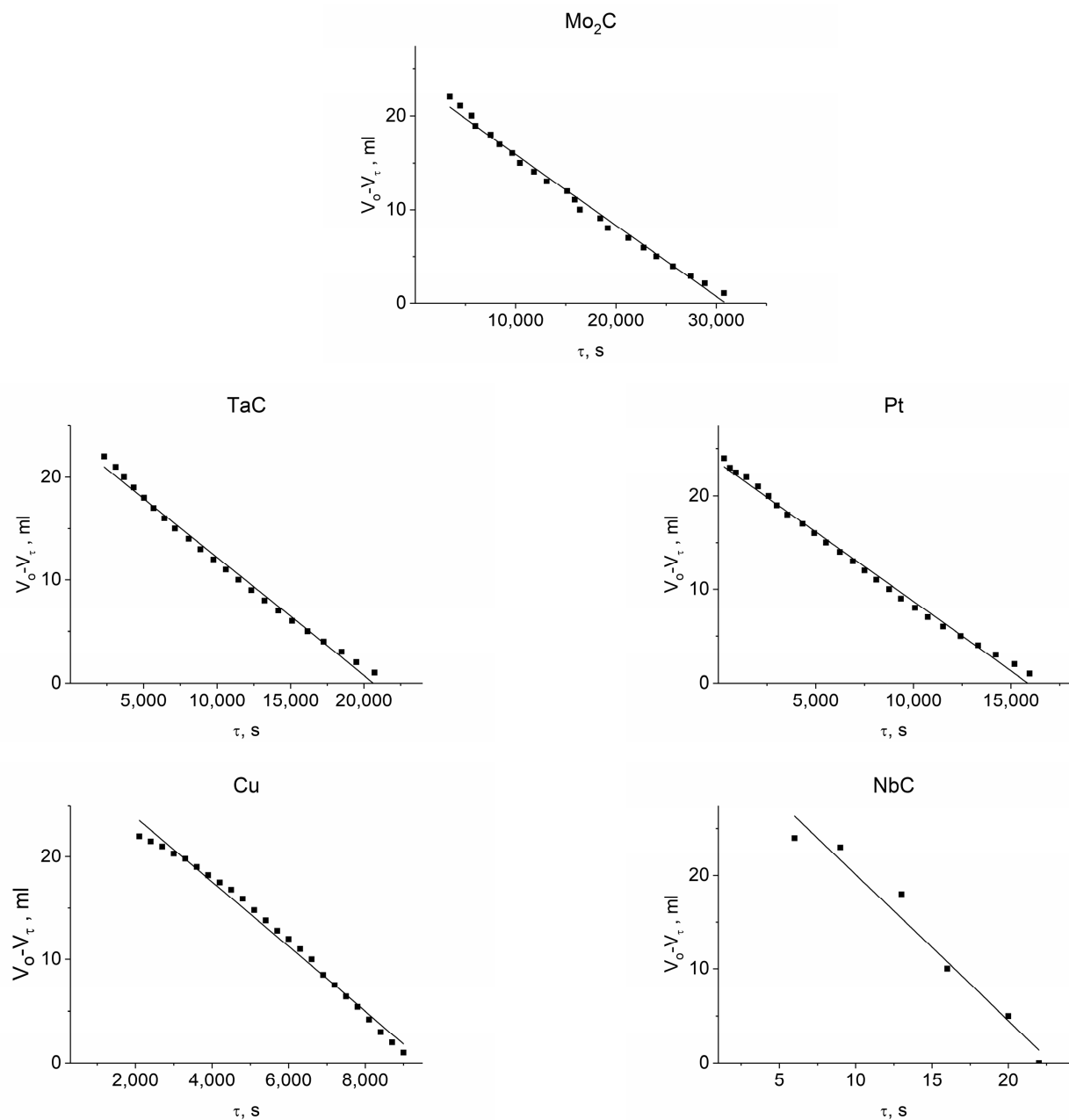


Figure 13. Zero-order kinetic dependencies of the electrocatalytic decomposition of H₂O₂, taken on the electrodes at the same temperature 303 K.

The activation energies of the studied H_2O_2 decomposition were calculated from experimental data obtained at different temperatures in steps of 10 K. Figure 13 shows the kinetic data at 303 K for all studied composites. Similar dependencies were also observed at higher temperatures, so only one example is presented in this article. It can be seen that the rate of electrocatalytic reaction of hydrogen peroxide decomposition increases in the following series: $\text{Mo}_2\text{C}/\text{C} < \text{TaC}/\text{C} < \text{Pt} < \text{Cu} < \text{NbC}/\text{C}$.

The obtained values of the rate constants for the hydrogen peroxide decomposition at different temperatures were used to calculate activation energies. It was found that the activation energy values for the $\text{Mo}_2\text{C}/\text{C}$, TaC/C , Pt, Cu and NbC/C electrodes are equal to 107.2, 82.2, 74.8, 48.2, and 37.1 kJ mol^{-1} , respectively.

It should be noted that the activation energy of the hydrogen peroxide decomposition process is given here from the general chemical point of view. Since it is impossible to reliably determine the value of the potential difference between the electrode surface and any point in the solution, we do not have a reliable method for the experimental determination of the activation energy for the specific electrode process. Therefore, the calculated activation energies are given for a formal decomposition process taking place on the anode.

It has been established that the reaction rate does not change over time, in accordance with the zero-order kinetic equation, which has no dependence on the concentration of reacting substances, and the diffusion rate to the surface of electrode is smaller than the rate of chemical transformation.

3.4. Electrochemical Synthesis of Gadolinium Borides Nanorods in Molten Salts

Highly pure rare earth metals and their refractory compounds with oxygen, carbon, nitrogen, and boron are widely used in special alloys in metallurgy, semiconductor electronics and laser techniques; they are used for production of permanent magnets, new types of catalysts, optical glasses, and hydrogen accumulators. Gadolinium boride is especially prospective in nuclear engineering for neutron adsorption. Nanomaterials based on gadolinium hexaboride are promising materials for modern technology due to their unique electric, magnetic, and optical properties. For example, GdB_6 nanorods are characterized by a very low electron work function (~ 1.5 eV), which makes this nanomaterial very interesting for the fabrication of point electron emitters. GdB_6 nanorods are strong light absorbers in the near infrared region, and they are transparent to visible light.

The traditional manufacturing of rare-earth borides is based on the direct reaction of pure initial components at high temperatures (up to 2700 K), which negatively affects the microstructure of the product. Electrochemical synthesis at moderate temperatures (973–1023 K) is a cost-effective alternative to direct reaction techniques and it has been successfully applied to the production of high-quality refractory borides. Electrochemical techniques provide not only the required stoichiometry and narrow size distribution of the product, but also the designated morphology. Prior to our studies, there was no information on the preparation of GdB_6 nanorods and nanowires in the literature.

For the electrochemical synthesis of GdB_6 it is necessary to know the electrochemical behavior of boron and gadolinium in their joint presence in the melt. Waves on the voltammogram in the $\text{NaCl-KCl-NaF-GdF}_3\text{-KBF}_4$ melt (Figure 14) reflected the boron reduction from BF_4^- complexes (R_B , the least negative wave at about -0.8 – -1.0 V) and gadolinium discharge on a boron deposit ($R_{\text{Gd-B}}$, at potentials -1.5 V and -1.8 V). The ascending section on the voltammogram corresponds to the discharge of gadolinium and alkali metal cations. Significant differences in the electroreduction potentials of boron and gadolinium allows us to make a reasonable assumption about the so-called “kinetic regime” [52] of their compound synthesis in the melt. Thus, the hexaboride can be synthesized only at current densities higher than the limiting current density for a more positive constituent (boron) discharge process. During co-deposition with boron, gadolinium reduced not on a silver surface, but on the layer of already deposited boron. The high depolarization value

of this process leads to the formation of boron-gadolinium compound at potentials near -1.5 V and -1.8 V.

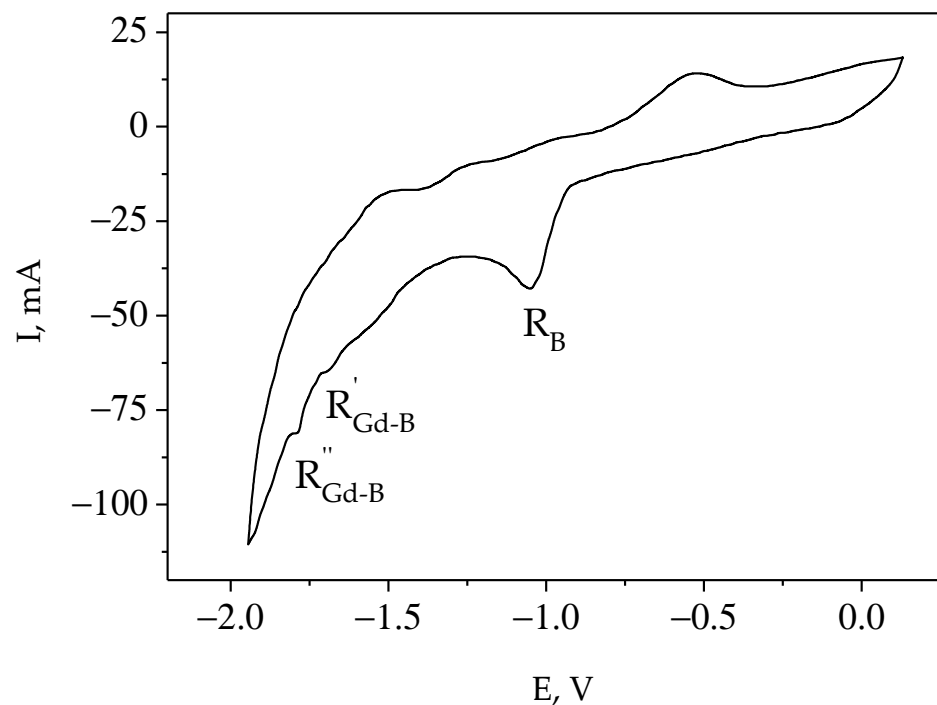


Figure 14. Voltammogram of the KCl-NaCl-NaF (10 wt.%)–GdF₃–KBF₄ (B/Gd = 2.6) melt, $C_{KBF_4} = 1.8 \times 10^{-5}$ mol cm⁻³, Ag—working electrode, $A = 0.5$ cm², GC—counter electrode, GC—quasi-reference electrode; $\nu = 0.5$ V s⁻¹, $T = 1023$ K.

Potentiostatic electrolysis (7 h duration) was carried out, at potentials -1.5 V and -1.8 V. The deposits were scraped off and any electrolyte adhering to the deposits were leached with a warm dilute HCl, then 2% NaOH, and finally washed with distilled water and ethanol. XRD analysis identified the products of electrolysis as gadolinium hexaboride [78]. At the potential of -1.5 V the gadolinium hexaboride was synthesized in the form of coral-like dendrites. Micro- and nanorods were obtained at the potential of -1.8 V (Figure 15). Along with nanorods, a GdB₆ nanowire was also formed on the cathode; the length of the nanostructure significantly exceeded its diameter, and, in some cases, the nanowire was bent. The intercalation mechanism was suggested for the formation of nanorods and nanowire [78].

3.5. Synthesis of One-Dimensional Nanostructures: Si and TaO Nanoneedles

One-dimensional nanomaterials, such as nanorods, nanotubes, nanowires, and nanofibers, are promising for catalysis and electrocatalysis [108]. Firstly, this is due to their large surface area with a high concentration of active centers [109]. Secondly, such nanostructures have a unique channel structure, which can be used as a fast pathway for the transfer of electric charges [110,111]. Finally, many adjacent one-dimensional nanostructures create a large number of pores and channels for the supply of reagents and escape of reaction products. Another important advantage of such structures is the possibility of obtaining them directly on the desired substrate without the use of additional binding agents [111].

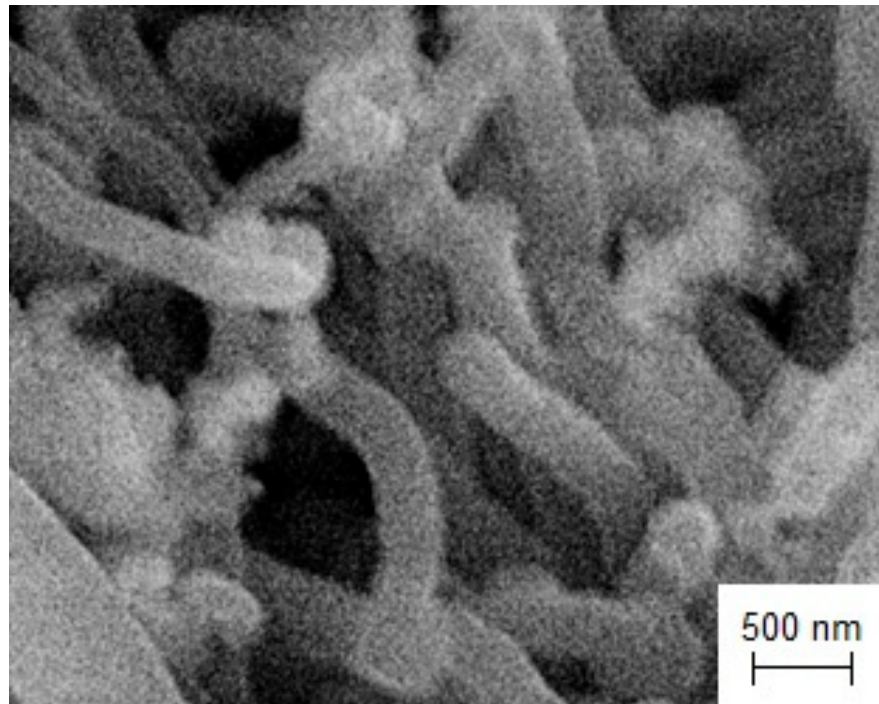


Figure 15. SEM image of the GdB_6 , synthesized in the $KCl-NaCl-NaF$ (10 wt.%)- GdF_3-KBF_4 melt at -1.8 V vs. GC quasi-reference electrode.

3.5.1. Electrochemical Synthesis of Si-Nanoneedles in Molten Salts

Silicon technology has created computers, cell phones, and other electronic devices [59,112]. The use of silicon nanoneedles for medical purposes is known [113,114], for example, to grow new blood vessels. Such nanoscale needles are involved in the delivery of genetic material to stimulate blood vessel growth and can deliver drugs directly to living cells.

Electrochemical methods of synthesis make it possible to produce nanoscale silicon, regulating its growth and the size of the final product [56].

A chloride-fluoride melt, $NaCl-KCl-NaF$ (10 wt.%)- K_2SiF_6 , was used for the production of silicon [115]. The cyclic voltammogram of this melt is presented in Figure 16 and in the cathodic semi-cycle, two electroreduction peaks R_1 and R_2 corresponding to $Si(IV)$ were registered.

Potentiostatic electrolysis at the first wave did not lead to the formation of solid product at the cathode, but after washing off the electrolyte remaining on the electrode, needle- and flake-form crystals were observed (Figure 17). The XRD analysis showed that the crystals correspond to elementary silicon [115].

Thus, the recharge process of $Si(IV)$ to $Si(II)$:



is accompanied by the disproportionation reaction [116]:



According to the XRD data, electrolysis at the potentials of the second wave led to the formation of large silicon crystals (Figure 18) during the electroreduction of $Si(II)$ to Si , and fine needle crystals were also observed due the disproportionation reaction (3).

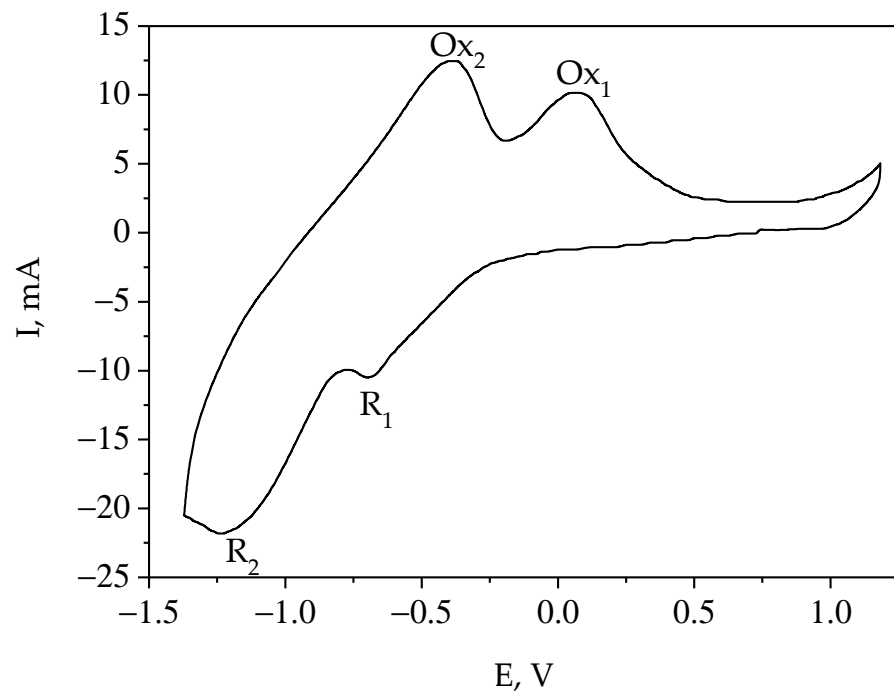


Figure 16. Cyclic voltammogram of the NaCl-KCl-NaF(10 wt.%)–K₂SiF₆ melt. Concentration of K₂SiF₆ is $6.87 \times 10^{-5} \text{ mol cm}^{-3}$; $v = 0.2 \text{ V s}^{-1}$; $T = 1023 \text{ K}$; $A = 0.162 \text{ cm}^2$. The quasi-reference electrode was the SU-2000 glassy carbon.

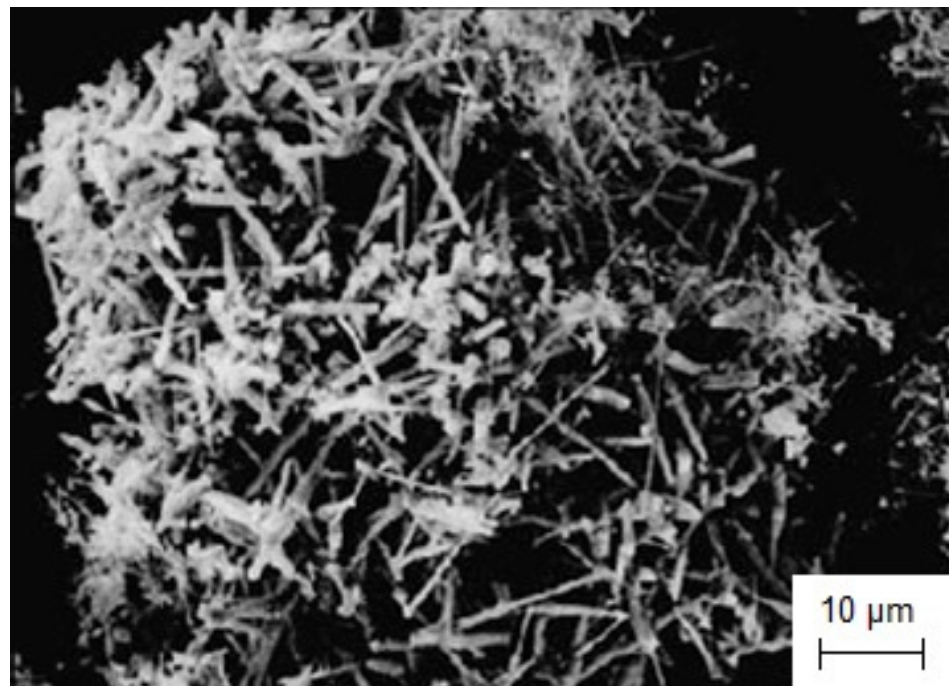


Figure 17. Needle and flake silicon crystals obtained during potentiostatic electrolysis at $E = -0.75 \text{ V}$ vs. the glassy carbon electrode, after rinsing the remaining electrolyte off the electrode after its removal from the melt.

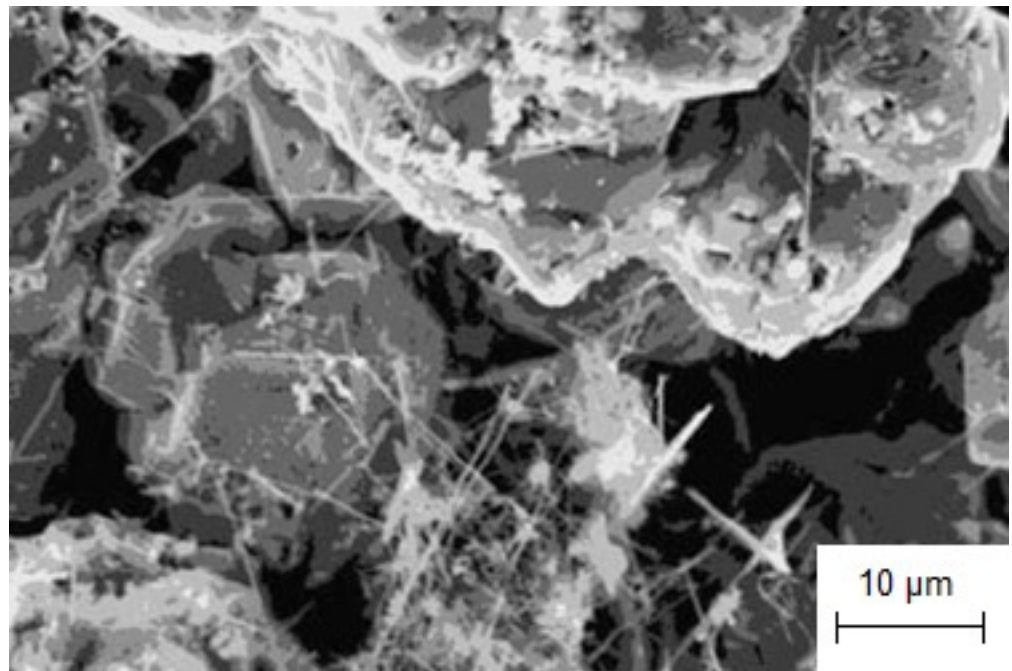


Figure 18. Electron microscope image of silicon crystals on a silver electrode obtained by potentiostatic electrolysis at $E = -1.2$ V vs. the glassy carbon electrode.

3.5.2. Obtaining of TaO Nanoneedles by Electroreduction of K_3TaOF_6 in Molten Salts

Tantalum monoxide can replace the tantalum pentoxide in high-density electric capacitors because of its high dielectric constant and low leakage current [117]. This material has been commercially integrated in capacitors which are used in computer dynamic random-access memory [118].

The formation of TaO was mentioned in several papers [119–123], but in [122,123] the electrocrystallization of tantalum monoxide was not confirmed by XRD analysis.

It was determined that during electroreduction of tantalum monoxofluoride complexes in the $CsCl-K_3TaOF_6$ melt, several phases containing tantalum are formed. The variation of cathodic products obtained at different parameters of electrolysis are presented in Figure 19. As can be seen from the diagrams in Figure 19, tantalum monoxide crystallized at the cathode with other tantalum compounds and did not form at a temperature of 1173 K. The micrograph of tantalum monoxide formed during electrolysis of the $CsCl-K_3TaOF_6$ melt is shown in Figure 20. It demonstrates that tantalum monoxide crystallizes at the cathode as nanoneedles up to 12,000 nm in length with a cross-section of ~ 100 nm.

Table 1 presents a brief summary of all functional coatings and nanomaterials considered in the present paper, the corresponding synthesis conditions in molten salts, and possible applications.

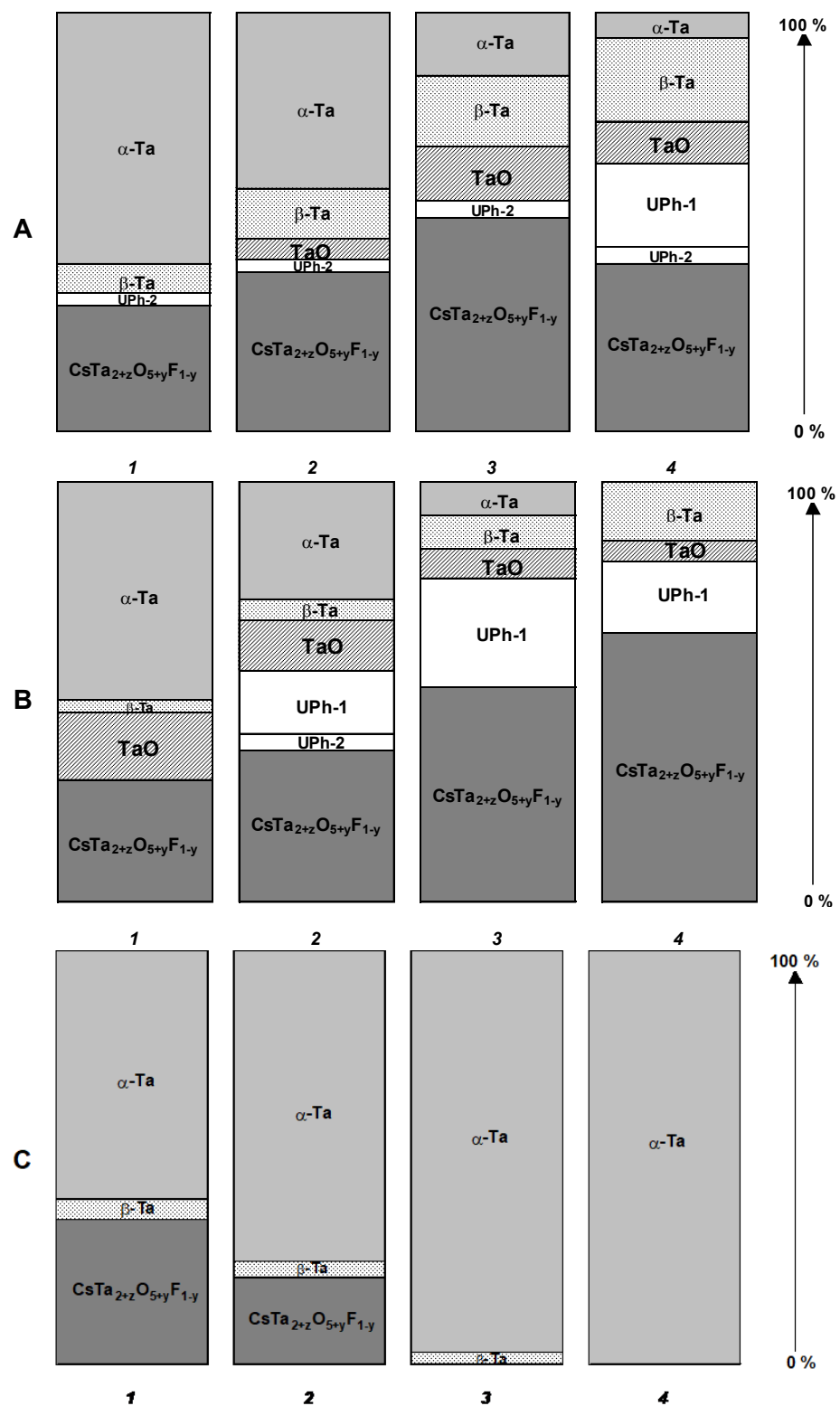


Figure 19. Diagrams of the phase composition of the cathodic products deposited at a current density of 0.15 A cm^{-2} at (A) 923 K, (B) 1023 K, (C) 1173 K. The concentration of K_3TaOF_6 in the $CsCl$ melt was (1) 1.25, (2) 2.5, (3) 5.0, and (4) 10.0 wt.%.



Figure 20. SEM image of TaO obtained by electrolysis of the CsCl-K₃TaOF₆ (2.5 wt.%) melt at 1023 K and a current density of 0.15 A cm⁻².

Table 1. Summary of electrochemical synthesis of functional coatings and nanomaterials in molten salts.

Molten Salt System	Deposition Regime	Experimental Condition	Substrate	Product	Possible Application
NaCl-KCl-Li ₂ CO ₃ -Na ₂ MoO ₄	Galvanostatic electrolysis	$i = 5 \text{ mA cm}^{-2}$ $\tau = 7 \text{ h}$ $T = 1123 \text{ K}$	Mo plate	Mo ₂ C nanostructured coating [84]	Catalyst for steam reforming reaction
NaCl-KCl-CrCl ₃ -Cr	Currentless transfer	$\tau = 8 \text{ h}$ $T = 1173 \text{ K}$	Steel St.3	Cr ₇ C ₃ coating [98,103]	Protective corrosion- and wear-resistant coating
NaCl-KCl-K ₂ TaF ₇ -Ta	Currentless transfer	$\tau = 8 \text{ h}$ $T = 1173 \text{ K}$	Steel St.3	TaC coating [103]	Protective corrosion- and wear-resistant coating
NaCl-KCl-K ₂ NbF ₇ -Nb	Currentless transfer	$\tau = 8 \text{ h}$ $T = 1173 \text{ K}$	Steel St.3	NbC coating [103]	Protective corrosion- and wear-resistant coating
NaCl-KCl-K ₂ TaF ₇ -Ta	Currentless transfer	$\tau = 24 \text{ h}$ $T = 1123 \text{ K}$	Carbon fibers	TaC coating [107]	Electrocatalyst for H ₂ O ₂ decomposition
NaCl-KCl-K ₂ NbF ₇ -Nb	Currentless transfer	$\tau = 24 \text{ h}$ $T = 1123 \text{ K}$	Carbon fibers	NbC coating [107]	Electrocatalyst for H ₂ O ₂ decomposition
NaCl-KCl-Na ₂ MoO ₄ -Mo	Currentless transfer	$\tau = 1 \text{ h}$ $T = 1123 \text{ K}$	Carbon fibers	Mo ₂ C crystals [107]	Electrocatalyst for H ₂ O ₂ decomposition
NaCl-KCl-NaF-GdF ₃ -KBF ₄	Potentiostatic electrolysis	$E = -1.8 \text{ V vs. GC}$ $\tau = 7 \text{ h}$ $T = 1023 \text{ K}$	Ag rod	GdB ₆ nanorods and nanowires [78]	Material for point electron emitters; Material for the neutron adsorption
NaCl-KCl-NaF-K ₂ SiF ₆	Potentiostatic electrolysis	$E = -0.75 \text{ V vs. GC}$ $\tau = 2 \text{ h}$ $T = 1023 \text{ K}$	Ag rod	Si nanoneedles [115]	Material for Li-ion batteries; Drug delivery into living cells
CsCl-K ₃ TaOF ₆	Galvanostatic electrolysis	$i = 0.15 \text{ A cm}^{-2}$ $\tau = 1 \text{ h}$ $T = 1023 \text{ K}$	Mo rod	TaO nanoneedles [80]	Material for high-density electric capacitors

4. Conclusions

The advantages of high-temperature electrochemical synthesis of nanostructured coatings and various nanomaterials in molten salts were demonstrated:

1. By electrochemical synthesis in molten salts, a new Mo₂C/Mo-based catalytic system for a low-temperature steam reforming reaction was obtained. The catalytic activity of this composition, produced by the simultaneous reduction of electroactive MoO₄²⁻ and CO₃²⁻ species, was three orders of magnitude higher than that of the bulk Mo₂C phase and commercial Cu-ZnO-Al₂O₃ catalyst.
2. The currentless transfer for the synthesis of nanoscale coatings of carbide refractory metals on substrates containing carbon was studied. It was shown that these coatings on steels increase corrosion resistance by several orders of magnitude and increase wear resistance by 3–5 times. Tests carried out by industrial facilities showed that the coatings of Cr₇C₃ or TaC on rubber-cutting knives made of St3 can improve their wear resistance and increase a tool lifetime by 2.0 (for Cr₇C₃) and 2.5 (for TaC) times.
3. It was found that NbC, TaC, and Mo₂C carbides deposited on carbon fibers by currentless transfer in molten salts can be used as highly active electrocatalysts for hydrogen peroxide decomposition. The kinetics of the electrocatalytic decomposition of H₂O₂ were studied and the following series of electrocatalytic activity was established: Mo₂C < TaC < Pt < Cu < NbC.
4. Using potentiostatic electrolysis, GdB₆ nanorods for different applications were synthesized in the KCl-NaCl-NaF(10 wt.%) -GdF₃-KBF₄ melt.
5. The synthesis of one-dimensional nanomaterials based on Si and TaO for application in modern electronic devices was discussed. Silicon nanoneedles were synthesized by potentiostatic electrolysis in the NaCl-KCl-NaF(10 wt.%) -K₂SiF₆ melt. The possibility to synthesize TaO using the CsCl-K₃TaOF₆ melt was shown. TaO crystallized at the cathode as nanoneedles, together with other tantalum compounds. It was found that TaO can be obtained by the electrolysis of molten salts only at temperatures below 1173 K.

Author Contributions: Investigation, Y.S., V.D. and A.D.; Supervision, S.K.; Visualization, Y.S., V.D. and A.D.; Writing—original draft, Y.S., V.D. and A.D.; Writing—review and editing, S.K. All authors have read and agreed to the published version of the manuscript.

Funding: This research received no external funding.

Institutional Review Board Statement: Not applicable.

Informed Consent Statement: Not applicable.

Data Availability Statement: The data presented in this study are available on request from the corresponding author.

Conflicts of Interest: The authors declare no conflict of interest.

References

1. Gleiter, H. Nanostructured Materials: Basic Concepts and Microstructure. *Acta Mater.* **2000**, *48*, 1–29. [[CrossRef](#)]
2. Nazar, L.F.; Goward, G.; Leroux, F.; Duncan, M.; Huang, H.; Kerr, T.; Gaubicher, J. Nanostructured Materials for Energy Storage. *Int. J. Inorg. Mater.* **2001**, *3*, 191–200. [[CrossRef](#)]
3. Hone, F.G.; Tegegne, N.A.; Andoshe, D.M. Advanced Materials for Energy Storage Devices. In *Electrode Materials for Energy Storage and Conversion*; CRC Press: Boca Raton, FL, USA, 2021; pp. 71–107. [[CrossRef](#)]
4. Kebede, M.A.; Ezema, F.I. Electrode Materials for Energy Storage and Conversion. In *Electrode Materials for Energy Storage and Conversion*; CRC Press: Boca Raton, FL, USA, 2021. [[CrossRef](#)]
5. Aoki, Y.; Tominaga, H.; Nagai, M. Hydrogenation of CO on Molybdenum and Cobalt Molybdenum Carbide Catalysts—Mass and Infrared Spectroscopy Studies. *Catal. Today* **2013**, *215*, 169–175. [[CrossRef](#)]
6. Ren, H.; Yu, W.; Saliccioli, M.; Chen, Y.; Huang, Y.; Xiong, K.; Vlachos, D.G.; Chen, J.G. Selective Hydrodeoxygenation of Biomass-Derived Oxygenates to Unsaturated Hydrocarbons Using Molybdenum Carbide Catalysts. *ChemSusChem* **2013**, *6*, 798–801. [[CrossRef](#)] [[PubMed](#)]

7. Schweitzer, N.M.; Schaidle, J.A.; Ezekoye, O.K.; Pan, X.; Linic, S.; Thompson, L.T. High Activity Carbide Supported Catalysts for Water Gas Shift. *J. Am. Chem. Soc.* **2011**, *133*, 2378–2381. [[CrossRef](#)]
8. Malyshev, V.; Uskova, N.; Shakhnin, D.; Lukashenko, T.; Antsibor, V.; Ustundag, Z. High-Temperature Electrochemical Synthesis of Nanostructured Coatings of Molybdenum (Tungsten)–Nickel (Cobalt) Alloys and Intermetallic Compounds. In *Selected Proceedings of the 5th International Conference Nanotechnology and Nanomaterials*; Springer: Berlin/Heidelberg, Germany, 2018; pp. 165–176. ISBN 9783319925660.
9. Zhang, W.; Hu, Y.; Ma, L.; Zhu, G.; Wang, Y.; Xue, X.; Chen, R.; Yang, S.; Jin, Z. Progress and Perspective of Electrocatalytic CO₂ Reduction for Renewable Carbonaceous Fuels and Chemicals. *Adv. Sci.* **2018**, *5*, 1700275. [[CrossRef](#)]
10. Hanus, M.J.; Harris, A.T. Nanotechnology Innovations for the Construction Industry. *Prog. Mater. Sci.* **2013**, *58*, 1056–1102. [[CrossRef](#)]
11. Zhai, W.; Srikanth, N.; Kong, L.B.; Zhou, K. Carbon Nanomaterials in Tribology. *Carbon N. Y.* **2017**, *119*, 150–171. [[CrossRef](#)]
12. Pottathara, Y.B.; Thomas, S.; Kalarikkal, N.; Grohens, Y.; Kokol, V. *Nanomaterials Synthesis*; Elsevier: Amsterdam, The Netherlands, 2019; ISBN 9780128157510.
13. Chen, X.; Mao, S.S. Titanium Dioxide Nanomaterials: Synthesis, Properties, Modifications and Applications. *Chem. Rev.* **2007**, *107*, 2891–2959. [[CrossRef](#)]
14. Chen, J.S.; Lou, X.W. SnO₂-Based Nanomaterials: Synthesis and Application in Lithium-Ion Batteries. *Small* **2013**, *9*, 1877–1893. [[CrossRef](#)]
15. Kolahalam, L.A.; Kasi Viswanath, I.V.; Diwakar, B.S.; Govindh, B.; Reddy, V.; Murthy, Y.L.N. Review on Nanomaterials: Synthesis and Applications. *Mater. Today Proc.* **2019**, *18*, 2182–2190. [[CrossRef](#)]
16. Sriondee, M.; Dungsuwan, W.; Thoutom, S. Synthesis and Characterization of Bi_{0.5}(Na_{1-x}K_x)_{0.5}TiO₃ Powders by Sol–Gel Combustion Method with Glycine Fuel. *Ceram. Int.* **2018**, *44*, S168–S171. [[CrossRef](#)]
17. Hao, S.; Lin, T.; Ning, S.; Qi, Y.; Deng, Z.; Wang, Y. Research on Cracking of SiO₂ Nanofilms Prepared by the Sol-Gel Method. *Mater. Sci. Semicond. Process.* **2019**, *91*, 181–187. [[CrossRef](#)]
18. Kasi Viswanath, I.V.; Murthy, Y.L.N.; Tata, K.R.; Singh, R. Synthesis and Characterization of Nano Ferrites by Citrate Gel Method. *Int. J. Chem. Sci.* **2013**, *11*, 64–72.
19. Ikesue, A.; Kinoshita, T.; Kamata, K.; Yoshida, K. Fabrication and Optical Properties of High-Performance Polycrystalline Nd:YAG Ceramics for Solid-State Lasers. *J. Am. Ceram. Soc.* **1995**, *78*, 1033–1040. [[CrossRef](#)]
20. Yu, S.; Jing, W.; Tang, M.; Xu, T.; Yin, W.; Kang, B. Fabrication of Nd:YAG Transparent Ceramics Using Powders Synthesized by Citrate Sol-Gel Method. *J. Alloys Compd.* **2019**, *772*, 751–759. [[CrossRef](#)]
21. Holland, B.T.; Blanford, C.F.; Do, T.; Stein, A. Synthesis of Highly Ordered, Three-Dimensional, Macroporous Structures of Amorphous or Crystalline Inorganic Oxides, Phosphates, and Hybrid Composites. *Chem. Mater.* **1999**, *11*, 795–805. [[CrossRef](#)]
22. Diwald, O.; Thompson, T.L.; Zubkov, T.; Goralski, E.G.; Walck, S.D.; Yates, J.T. Photochemical Activity of Nitrogen-Doped Rutile TiO₂(110) in Visible Light. *J. Phys. Chem. B* **2004**, *108*, 6004–6008. [[CrossRef](#)]
23. Sasaki, T.; Watanabe, M.; Hashizume, H.; Yamada, H.; Nakazawa, H. Macromolecule-like Aspects for a Colloidal Suspension of an Exfoliated Titanate. Pairwise Association of Nanosheets and Dynamic Reassembling Process Initiated from It. *J. Am. Chem. Soc.* **1996**, *118*, 8329–8335. [[CrossRef](#)]
24. Schlüter, M.; Hentzel, T.; Suarez, C.; Koch, M.; Lorenz, W.G.; Böhm, L.; Düring, R.A.; Koinig, K.A.; Bunge, M. Synthesis of Novel Palladium(0) Nanocatalysts by Microorganisms from Heavy-Metal-Influenced High-Alpine Sites for Dehalogenation of Polychlorinated Dioxins. *Chemosphere* **2014**, *117*, 462–470. [[CrossRef](#)]
25. Anderson, S.H.; Chung, D.D.L. Exfoliation of Single Crystal Graphite and Graphite Fibers Intercalated with Halogens. *Synth. Met.* **1983**, *8*, 343–349. [[CrossRef](#)]
26. Sharma, N.; Sharma, V.; Sharma, S.K.; Sachdev, K. Gas Sensing Behaviour of Green Synthesized Reduced Graphene Oxide (RGO) for H₂ and NO. *Mater. Lett.* **2019**, *236*, 444–447. [[CrossRef](#)]
27. Kadam, R.H.; Desai, K.; Shinde, V.S.; Hashim, M.; Shirsath, S.E. Influence of Gd³⁺ Ion Substitution on the MnCrFeO₄ for Their Nanoparticle Shape Formation and Magnetic Properties. *J. Alloys Compd.* **2016**, *657*, 487–494. [[CrossRef](#)]
28. Shi, Y.; Li, H.; Li, L.J. Recent Advances in Controlled Synthesis of Two-Dimensional Transition Metal Dichalcogenides via Vapour Deposition Techniques. *Chem. Soc. Rev.* **2015**, *44*, 2744–2756. [[CrossRef](#)] [[PubMed](#)]
29. Ismach, A.; Druzgalski, C.; Penwell, S.; Schwartzberg, A.; Zheng, M.; Javey, A.; Bokor, J.; Zhang, Y. Direct Chemical Vapor Deposition of Graphene on Dielectric Surfaces. *Nano Lett.* **2010**, *10*, 1542–1548. [[CrossRef](#)]
30. Kim, K.K.; Hsu, A.; Jia, X.; Kim, S.M.; Shi, Y.; Hofmann, M.; Nezich, D.; Rodriguez-Nieva, J.F.; Dresselhaus, M.; Palacios, T.; et al. Synthesis of Monolayer Hexagonal Boron Nitride on Cu Foil Using Chemical Vapor Deposition. *Nano Lett.* **2012**, *12*, 161–166. [[CrossRef](#)]
31. Saito, T.; Chiba, H.; Ito, T.; Ogino, T. Growth of Carbon Hybrid Materials by Grafting on Pre-Grown Carbon Nanotube Surfaces. *Carbon N. Y.* **2010**, *48*, 1305–1311. [[CrossRef](#)]
32. Xie, W.; Pang, Z.; Fan, J.; Song, H.; Jiang, F.; Yuan, H.; Li, J.; Ji, Z.; Han, S. Structural Properties of Alq₃ Nanocrystals Prepared by Physical Vapor Deposition and Facile Solution Method. *Int. J. Mod. Phys. B* **2015**, *29*, 1542042. [[CrossRef](#)]
33. Maleki, A. Green Oxidation Protocol: Selective Conversions of Alcohols and Alkenes to Aldehydes, Ketones and Epoxides by Using a New Multiwall Carbon Nanotube-Based Hybrid Nanocatalyst via Ultrasound Irradiation. *Ultrason. Sonochem.* **2018**, *40*, 460–464. [[CrossRef](#)]

34. Xu, H.; Suslick, K.S. Sonochemical Synthesis of Highly Fluorescent Ag Nanoclusters. *ACS Nano* **2010**, *4*, 3209–3214. [[CrossRef](#)] [[PubMed](#)]
35. Morel, A.L.; Nikitenko, S.I.; Gionnet, K.; Wattiaux, A.; Lai-Kee-Him, J.; Labrugere, C.; Chevalier, B.; Deleris, G.; Petibois, C.; Brisson, A.; et al. Sonochemical Approach to the Synthesis of Fe₃O₄@SiO₂ Core–Shell Nanoparticles with Tunable Properties. *ACS Nano* **2008**, *2*, 847–856. [[CrossRef](#)]
36. Gedanken, A. Using Sonochemistry for the Fabrication of Nanomaterials. *Ultrason. Sonochem.* **2004**, *11*, 47–55. [[CrossRef](#)]
37. Bang, J.H.; Suslick, K.S. Applications of Ultrasound to the Synthesis of Nanostructured Materials. *Adv. Mater.* **2010**, *22*, 1039–1059. [[CrossRef](#)]
38. Zuo, P.; Lu, X.; Sun, Z.; Guo, Y.; He, H. A Review on Syntheses, Properties, Characterization and Bioanalytical Applications of Fluorescent Carbon Dots. *Microchim. Acta* **2016**, *183*, 519–542. [[CrossRef](#)]
39. Gawande, M.B.; Shelke, S.N.; Zboril, R.; Varma, R.S. Microwave-Assisted Chemistry: Synthetic Applications for Rapid Assembly of Nanomaterials and Organics. *Acc. Chem. Res.* **2014**, *47*, 1338–1348. [[CrossRef](#)] [[PubMed](#)]
40. Baghbanzadeh, M.; Carbone, L.; Cozzoli, P.D.; Kappe, C.O. Microwave-Assisted Synthesis of Colloidal Inorganic Nanocrystals. *Angew. Chem.-Int. Ed.* **2011**, *50*, 11312–11359. [[CrossRef](#)]
41. Bilecka, I.; Niederberger, M. Microwave Chemistry for Inorganic Nanomaterials Synthesis. *Nanoscale* **2010**, *2*, 1358–1374. [[CrossRef](#)] [[PubMed](#)]
42. Ustarroz, J.; Hammons, J.A.; Altantzis, T.; Hubin, A.; Bals, S.; Terryn, H. A Generalized Electrochemical Aggregative Growth Mechanism. *J. Am. Chem. Soc.* **2013**, *135*, 11550–11561. [[CrossRef](#)]
43. Yin, Y.; Jin, Z.; Hou, F. Enhanced Solar Water-Splitting Efficiency Using Core/Sheath Heterostructure CdS/TiO₂ Nanotube Arrays. *Nanotechnology* **2007**, *18*, 495608. [[CrossRef](#)]
44. Zhu, T.; Chong, M.N.; Chan, E.S. Nanostructured Tungsten Trioxide Thin Films Synthesized for Photoelectrocatalytic Water Oxidation: A Review. *ChemSusChem* **2014**, *7*, 2974–2997. [[CrossRef](#)] [[PubMed](#)]
45. Mudring, A.V.; Tang, S. Ionic Liquids for Lanthanide and Actinide Chemistry. *Eur. J. Inorg. Chem.* **2010**, *2010*, 2569–2581. [[CrossRef](#)]
46. Chou, S.; Cheng, F.; Chen, J. Electrodeposition Synthesis and Electrochemical Properties of Nanostructured γ -MnO₂ Films. *J. Power Sources* **2006**, *162*, 727–734. [[CrossRef](#)]
47. Logeeswaran, V.J.; Kobayashi, N.P.; Islam, M.S.; Wu, W.; Chaturvedi, P.; Fang, N.X.; Wang, S.Y.; Williams, R.S. Ultrasoft Silver Thin Films Deposited with a Germanium Nucleation Layer. *Nano Lett.* **2009**, *9*, 178–182. [[CrossRef](#)] [[PubMed](#)]
48. Tepavcevic, S.; Xiong, H.; Stamenkovic, V.R.; Zuo, X.; Balasubramanian, M.; Prakapenka, V.B.; Johnson, C.S.; Rajh, T. Nanostructured Bilayered Vanadium Oxide Electrodes for Rechargeable Sodium-Ion Batteries. *ACS Nano* **2012**, *6*, 530–538. [[CrossRef](#)]
49. Abo-Hamad, A.; Hayyan, M.; AlSaadi, M.A.H.; Hashim, M.A. Potential Applications of Deep Eutectic Solvents in Nanotechnology. *Chem. Eng. J.* **2015**, *273*, 551–567. [[CrossRef](#)]
50. Shiddiky, M.J.A.; Torriero, A.A.J. Application of Ionic Liquids in Electrochemical Sensing Systems. *Biosens. Bioelectron.* **2011**, *26*, 1775–1787. [[CrossRef](#)] [[PubMed](#)]
51. Eftekhari, A. *Nanostructured Materials in Electrochemistry*; Wiley: Hoboken, NJ, USA, 2008.
52. Krishtalik, L.I. *Electrode Reactions. Mechanism of Elementary Act*; Nauka: Moscow, Russia, 1982.
53. Islam, M.M.; Abdellaoui, I.; Moslah, C.; Sakurai, T.; Ksibi, M.; Hamzaoui, S.; Akimoto, K. Electrodeposition and Characterization of Silicon Films Obtained through Electrochemical Reduction of SiO₂ Nanoparticles. *Thin Solid Film.* **2018**, *654*, 1–10. [[CrossRef](#)]
54. Zou, X.; Ji, L.; Ge, J.; Sadoway, D.R.; Yu, E.T.; Bard, A.J. Electrodeposition of Crystalline Silicon Films from Silicon Dioxide for Low-Cost Photovoltaic Applications. *Nat. Commun.* **2019**, *10*, 5772. [[CrossRef](#)]
55. Weng, W.; Xiao, W. Electrodeposited Silicon Nanowires from Silica Dissolved in Molten Salts as a Binder-Free Anode for Lithium-Ion Batteries. *ACS Appl. Energy Mater.* **2019**, *2*, 804–813. [[CrossRef](#)]
56. Laptev, M.V.; Isakov, A.V.; Grishenkova, O.V.; Vorob'ev, A.S.; Khudorozhkova, A.O.; Akashev, L.A.; Zaikov, Y.P. Electrodeposition of Thin Silicon Films from the KF-KCl-KI-K₂SiF₆ Melt. *J. Electrochem. Soc.* **2020**, *167*, 042506. [[CrossRef](#)]
57. Zou, X.; Ji, L.; Pang, Z.; Xu, Q.; Lu, X. Continuous Electrodeposition of Silicon and Germanium Micro/nanowires from Their Oxides Precursors in Molten Salt. *J. Energy Chem.* **2020**, *44*, 147–153. [[CrossRef](#)]
58. Yasko, O.; Shakhnin, D.B.; Gab, A.; Malyshev, V.; Gaune-Escard, M. Electrodeposition of Nanostructured Silicon Coatings onto Different Materials from Halide and Halide–Oxide Melts. In *Springer Proceedings in Physics*; Springer Science and Business Media Deutschland GmbH: Berlin, Germany, 2021; Volume 246, pp. 231–235. ISBN 9783030519049.
59. Gevel, T.; Zhuk, S.; Leonova, N.; Leonova, A.; Trofimov, A.; Suzdaltsev, A.; Zaikov, Y. Electrochemical Synthesis of Nano-Sized Silicon from KCl–K₂SiF₆ Melts for Powerful Lithium-Ion Batteries. *Appl. Sci.* **2021**, *11*, 10927. [[CrossRef](#)]
60. Wang, F.; Ma, Y.; Li, P.; Peng, C.; Yin, H.; Li, W.; Wang, D. Electrochemical Conversion of Silica Nanoparticles to Silicon Nanotubes in Molten Salts: Implications for High-Performance Lithium-Ion Battery Anode. *ACS Appl. Nano Mater.* **2021**, *4*, 7028–7036. [[CrossRef](#)]
61. Jing, S.; Xiao, J.; Shen, Y.; Hong, B.; Gu, D.; Xiao, W. Silicate-Mediated Electrolytic Silicon Nanotube from Silica in Molten Salts. *Small* **2022**, *18*, 2203251. [[CrossRef](#)]
62. Rezaei, A.; Kamali, A.R. Green Production of Carbon Nanomaterials in Molten Salts, Mechanisms and Applications. *Diam. Relat. Mater.* **2018**, *83*, 146–161. [[CrossRef](#)]

63. Hu, L.; Song, Y.; Ge, J.; Zhu, J.; Jiao, S. Capture and Electrochemical Conversion of CO₂ to Ultrathin Graphite Sheets in CaCl₂-Based Melts. *J. Mater. Chem. A* **2015**, *3*, 21211–21218. [[CrossRef](#)]
64. Wu, H.; Li, Z.; Ji, D.; Liu, Y.; Li, L.; Yuan, D.; Zhang, Z.; Ren, J.; Lefler, M.; Wang, B.; et al. One-Pot Synthesis of Nanostructured Carbon Materials from Carbon Dioxide via Electrolysis in Molten Carbonate Salts. *Carbon N. Y.* **2016**, *106*, 208–217. [[CrossRef](#)]
65. Novoselova, I.A.; Oliynyk, N.F.; Volkov, S.V. Electrolytic Production of Carbon Nano-Tubes in Chloride-Oxide Melts under Carbon Dioxide Pressure. In *Hydrogen Materials Science and Chemistry of Carbon Nanomaterials*; Springer: Dordrecht, The Netherlands, 2007; pp. 459–465. ISBN 1402055129.
66. Ijje, H.V.; Lawrence, R.C.; Chen, G.Z. Carbon Electrodeposition in Molten Salts: Electrode Reactions and Applications. *RSC Adv.* **2014**, *4*, 35808–35817. [[CrossRef](#)]
67. Mao, X.; Yan, Z.; Sheng, T.; Gao, M.; Zhu, H.; Xiao, W.; Wang, D. Characterization and Adsorption Properties of the Electrolytic Carbon Derived from CO₂ Conversion in Molten Salts. *Carbon N. Y.* **2017**, *111*, 162–172. [[CrossRef](#)]
68. Kushkhov, K.B.; Ligidova, M.N.; Ali, J.Z.; Khotov, A.A.; Tlenkopachev, M.R.; Karatsukova, R.K. Electrochemical Processes in Molten Alkaline Metal Carbonates under Carbon Dioxide Overpressure. *Russ. Metall.* **2021**, *2021*, 141–150. [[CrossRef](#)]
69. Wang, M.; Kim, Y.; Zhang, L.; Seong, W.K.; Kim, M.; Chatterjee, S.; Wang, M.; Li, Y.; Bakharev, P.V.; Lee, G.; et al. Controllable Electrodeposition of Ordered Carbon Nanowalls on Cu(111) Substrates. *Mater. Today* **2022**, *57*, 75–83. [[CrossRef](#)]
70. Kumar, K.; Mondal, S. Fabrication and Characterisation of Carbon Nanotube Reinforced Copper Matrix Nanocomposites. *Can. Metall. Q.* **2022**, *61*, 77–84. [[CrossRef](#)]
71. Groult, H.; Le Van, K.; Lantelme, F. Electrodeposition of Carbon-Metal Powders in Alkali Carbonate Melts. *J. Electrochem. Soc.* **2014**, *161*, D3130–D3138. [[CrossRef](#)]
72. Hu, L.; Song, Y.; Ge, J.; Zhu, J.; Han, Z.; Jiao, S. Electrochemical Deposition of Carbon Nanotubes from CO₂ in CaCl₂–NaCl-Based Melts. *J. Mater. Chem. A* **2017**, *5*, 6219–6225. [[CrossRef](#)]
73. Xu, Q.; Schwandt, C.; Chen, G.Z.; Fray, D.J. Electrochemical Investigation of Lithium Intercalation into Graphite from Molten Lithium Chloride. *J. Electroanal. Chem.* **2002**, *530*, 16–22. [[CrossRef](#)]
74. Kamali, A.R. Nanocatalytic Conversion of CO₂ into Nanodiamonds. *Carbon N. Y.* **2017**, *123*, 205–215. [[CrossRef](#)]
75. Yasko, O.; Malyshev, V.; Gab, A.; Lukashenko, T. Joint Electroreduction of Carbonate and Tungstate Ions as the Base for Tungsten Carbide Nanopowders Synthesis in Ionic Melts. In *Springer Proceedings in Physics*; Springer Science and Business Media, LLC: Berlin, Germany, 2019; Volume 221, pp. 397–402. ISBN 9783030177584.
76. Malyshev, V.; Gab, A.; Shakhnin, D.; Lukashenko, T.; Ishtvanik, O.; Gaune-Escard, M. High-Temperature Electrochemical Synthesis of Nanopowders of Tungsten Carbide in Ionic Melts. In *Springer Proceedings in Physics*; Springer Science and Business Media, LLC: Berlin, Germany, 2018; Volume 214, pp. 311–321. ISBN 9783319925660.
77. Kushkhov, K.B.; Kardanov, A.L.; Adamokova, M.N. Electrochemical Synthesis of Binary Molybdenum-Tungsten Carbides (Mo,W)₂C from Tungstate-Molybdate-Carbonate Melts. *Russ. Metall.* **2013**, *2013*, 79–85. [[CrossRef](#)]
78. Bukatova, G.A.; Kuznetsov, S.A. Electrolysis of Gadolinium Hexaboride Nanotubes. *Electrochem. Commun.* **2005**, *7*, 637–641. [[CrossRef](#)]
79. Kuznetsov, S.A.; Kremenetsky, V.G.; Popova, A.V.; Kremenetskaya, O.V.; Kalinnikov, V.T. Unusual Effect of the Second Coordination Sphere on the Standard Charge Transfer Rate Constants for the Nb(V)/Nb(IV) Redox Couple in Chloride–Fluoride Melts. *Dokl. Phys. Chem.* **2009**, *428*, 209–212. [[CrossRef](#)]
80. Grinevitch, V.V.; Kuznetsov, S.A.; Arakcheeva, A.A.; Olyunina, T.V.; Schönleber, A.; Gaune-Escard, M. Electrode and Chemical Reactions during Electrodeposition of Tantalum Products in CsCl Melt. *Electrochim. Acta* **2006**, *51*, 6563–6571. [[CrossRef](#)]
81. Kuznetsov, S.A.; Rebrov, E.V.; Mies, M.J.M.; de Croon, M.H.J.M.; Schouten, J.C. Synthesis of Protective Mo–Si–B Coatings in Molten Salts and Their Oxidation Behavior in an Air–Water Mixture. *Surf. Coat. Technol.* **2006**, *201*, 971–978. [[CrossRef](#)]
82. Grinevitch, V.V.; Arakcheeva, A.V.; Kuznetsov, S.A. Tantalum Metal of Peculiar Crystal Lattice (b-Ta) as Creation of Electrocrystallization from Molten Salts. In *International Symposium on Ionic Liquids*; DTU Research Database: Carry le Rouet, France, 2003; pp. 277–285.
83. Dubrovskiy, A.R.; Makarova, O.V.; Kuznetsov, S.A. Effect of the Molybdenum Substrate Shape on Mo₂C Coating Electrodeposition. *Coatings* **2018**, *8*, 442. [[CrossRef](#)]
84. Dubrovskii, A.R.; Kuznetsov, S.A.; Rebrov, E.V.; Schouten, J.C. Catalytic Coatings of New Generation Based on Mo₂C and a Microstructured Reactor for Steam Conversion of Carbon Monoxide. *Russ. J. Appl. Chem.* **2014**, *87*, 601–607. [[CrossRef](#)]
85. Dubrovskiy, A.R.; Okunev, M.A.; Makarova, O.V.; Kuznetsov, S.A. Superconducting Niobium Coatings Deposited on Spherical Substrates in Molten Salts. *Coatings* **2018**, *8*, 213. [[CrossRef](#)]
86. Patt, J.; Moon, D.J.; Phillips, C.; Thompson, L. Molybdenum Carbide Catalysts for Water-Gas Shift. *Catal. Lett.* **2000**, *65*, 193–195. [[CrossRef](#)]
87. Derakhshandeh, M.R.; Eshraghi, M.J.; Razavi, M. Recent Developments in the New Generation of Hard Coatings Applied on Cemented Carbide Cutting Tools. *Int. J. Refract. Met. Hard Mater.* **2023**, *111*, 106077. [[CrossRef](#)]
88. Lee, C.; Danon, Y.; Mulligan, C. Characterization of Niobium, Tantalum and Chromium Sputtered Coatings on Steel Using Eddy Currents. *Surf. Coat. Technol.* **2005**, *200*, 2547–2556. [[CrossRef](#)]
89. Lee, Y.J.; Lee, T.H.; Kim, D.Y.; Nersisyan, H.H.; Han, M.H.; Kang, K.S.; Bae, K.K.; Shin, Y.J.; Lee, J.H. Microstructural and Corrosion Characteristics of Tantalum Coatings Prepared by Molten Salt Electrodeposition. *Surf. Coat. Technol.* **2013**, *235*, 819–826. [[CrossRef](#)]

90. Emsley, J. *Nature's Building Blocks: An A-Z Guide to the Elements*; Oxford University Press: Oxford, UK, 2003.
91. Baklanova, N.I.; Zima, T.M.; Boronin, A.I.; Kosheev, S.V.; Titov, A.T.; Isaeva, N.V.; Graschenkov, D.V.; Solntsev, S.S. Protective Ceramic Multilayer Coatings for Carbon Fibers. *Surf. Coat. Technol.* **2006**, *201*, 2313–2319. [[CrossRef](#)]
92. Wang, S.-C.; Lin, H.-T.; Nayak, P.K.; Chang, S.-Y.; Huang, J.-L. Carbothermal Reduction Process for Synthesis of Nanosized Chromium Carbide via Metal-Organic Vapor Deposition. *Thin Solid Film.* **2010**, *518*, 7360–7365. [[CrossRef](#)]
93. Sen, S. Influence of Chromium Carbide Coating on Tribological Performance of Steel. *Mater. Des.* **2006**, *27*, 85–91. [[CrossRef](#)]
94. Gómez, M.A.; Romero, J.; Lousa, A.; Esteve, J. Tribological Performance of Chromium/Chromium Carbide Multilayers Deposited by r.f. Magnetron Sputtering. *Surf. Coat. Technol.* **2005**, *200*, 1819–1824. [[CrossRef](#)]
95. Cintho, O.M.; Favilla, E.A.P.; Capocchi, J.D.T. Mechanical–Thermal Synthesis of Chromium Carbides. *J. Alloys Compd.* **2007**, *439*, 189–195. [[CrossRef](#)]
96. Esteve, J.; Romero, J.; Gómez, M.; Lousa, A. Cathodic Chromium Carbide Coatings for Molding Die Applications. *Surf. Coat. Technol.* **2004**, *188–189*, 506–510. [[CrossRef](#)]
97. Shatinsky, V.D.; Nesterenko, F.I. *Protecting Diffusional Coatings*; Naukova Dumka: Kiev, Ukraine, 1988.
98. Stulov, Y.V.; Kuznetsov, S.A. Synthesis of Chromium Carbide Coatings on Carbon Steels in Molten Salts and Their Properties. *Glas. Phys. Chem.* **2014**, *40*, 324–328. [[CrossRef](#)]
99. Ilyushchenko, N.G.; Afinogenov, A.I.; Shurov, N.I. *Metal Interactions in Ionic Melts*; Nauka: Moscow, Russia, 1991.
100. Novokreshchenov, Y.V.; Petenev, O.S.; Kositsyn, Y.N. Influence of anodic polarization on spontaneous transfer of metals from salt melts onto articles for protection by thermal chemical treatment. *J. Appl. Chem. USSR* **1986**, *59*, 2492–2494.
101. Malyshev, V.V.; Shakhnin, D.B.; Hab, A.; Kublanovs'kyi, V.S.; Schuster, D. Synthesis of Chromium Silicides in Ionic Melts. *Mater. Sci.* **2020**, *55*, 745–757. [[CrossRef](#)]
102. Kovalevskii, A.V.; El'Kin, O.V. The Electrochemical Properties of LiCl-KCl Melt Held in Contact with Samarium. *Russ. J. Phys. Chem. A* **2011**, *85*, 499–502. [[CrossRef](#)]
103. Stulov, Y.V.; Dolmatov, V.S.; Dubrovskii, A.R.; Kuznetsov, S.A. Coatings by Refractory Metal Carbides: Deposition from Molten Salts, Properties, Application. *Russ. J. Appl. Chem.* **2017**, *90*, 676–683. [[CrossRef](#)]
104. Böhm, H. Adsorption Und Anodische Oxydation von Wasserstoff an Wolframcarbide. *Electrochim. Acta* **1970**, *15*, 1273–1280. [[CrossRef](#)]
105. Goti, A.; Cardona, F. Hydrogen Peroxide in Green Oxidation Reactions: Recent Catalytic Processes. In *Green Chemical Reactions*; Springer: Dordrecht, The Netherlands, 2008; pp. 191–212. [[CrossRef](#)]
106. Bloom, H. *Electrochemistry: The Past Thirty and the Next Thirty Years*; Springer: Berlin/Heidelberg, Germany, 2012.
107. Dolmatov, V.S.; Kuznetsov, S.A. Synthesis of Refractory Metal Carbides on Carbon Fibers in Molten Salts and Their Electrocatalytic Properties. *J. Electrochem. Soc.* **2021**, *168*, 122501. [[CrossRef](#)]
108. Guan, A.; Yang, C.; Quan, Y.; Shen, H.; Cao, N.; Li, T.; Ji, Y.; Zheng, G. One-Dimensional Nanomaterial Electrocatalysts for CO₂ Fixation. *Chem.-An Asian J.* **2019**, *14*, 3969–3980. [[CrossRef](#)]
109. Peng, S.; Li, L.; Kong Yoong Lee, J.; Tian, L.; Srinivasan, M.; Adams, S.; Ramakrishna, S. Electrospun Carbon Nanofibers and Their Hybrid Composites as Advanced Materials for Energy Conversion and Storage. *Nano Energy* **2016**, *22*, 361–395. [[CrossRef](#)]
110. Wang, H.G.; Yuan, S.; Ma, D.L.; Zhang, X.B.; Yan, J.M. Electrospun Materials for Lithium and Sodium Rechargeable Batteries: From Structure Evolution to Electrochemical Performance. *Energy Environ. Sci.* **2015**, *8*, 1660–1681. [[CrossRef](#)]
111. Jin, T.; Han, Q.; Wang, Y.; Jiao, L.; Jin, T.; Han, Q.; Wang, Y.; Jiao, L. 1D Nanomaterials: Design, Synthesis, and Applications in Sodium-Ion Batteries. *Small* **2018**, *14*, 1703086. [[CrossRef](#)] [[PubMed](#)]
112. Kohmura, Y.; Zhakhovskiy, V.; Takei, D.; Suzuki, Y.; Takeuchi, A.; Inoue, I.; Inubushi, Y.; Inogamov, N.; Ishikawa, T.; Yabashi, M. Nano-Structuring of Multi-Layer Material by Single x-Ray Vortex Pulse with Femtosecond Duration. *Appl. Phys. Lett.* **2018**, *112*, 123103. [[CrossRef](#)]
113. Salih, O.S.; Al-Akkam, E.J. Microneedles as A Magical Technology to Facilitate Transdermal Drug Delivery: A Review Article. *Int. J. Drug Deliv. Technol.* **2022**, *12*, 896–901. [[CrossRef](#)]
114. Pan, J.; Low, K.L.; Ghosh, J.; Jayavelu, S.; Ferdaus, M.M.; Lim, S.Y.; Zamburg, E.; Li, Y.; Tang, B.; Wang, X.; et al. Transfer Learning-Based Artificial Intelligence-Integrated Physical Modeling to Enable Failure Analysis for 3 Nanometer and Smaller Silicon-Based CMOS Transistors. *ACS Appl. Nano Mater.* **2021**, *4*, 6903–6915. [[CrossRef](#)]
115. Kuznetsova, S.V.; Dolmatov, V.S.; Kuznetsov, S.A. Voltammetric Study of Electroreduction of Silicon Complexes in a Chloride-Fluoride Melt. *Russ. J. Electrochem.* **2009**, *45*, 742–748. [[CrossRef](#)]
116. Nicholson, R.S.; Shain, I. Theory of Stationary Electrode Polarography: Single Scan and Cyclic Methods Applied to Reversible, Irreversible, and Kinetic Systems. *Anal. Chem.* **1964**, *36*, 706–723. [[CrossRef](#)]
117. Nakamura, Y.; Asano, I.; Hiratani, M.; Saito, T.; Goto, H. Oxidation-Resistant Amorphous TaN Barrier for MIM-Ta₂O₅ Capacitors in Giga-Bit DRAMs. In Proceedings of the 2001 Symposium on VLSI Technology. Digest of Technical Papers, Kyoto, Japan, 12–14 June 2001; pp. 39–40. [[CrossRef](#)]
118. Matsui, Y.; Hiratani, M.; Kimura, S.; Asano, I. Combining Ta₂O₅ and Nb₂O₅ in Bilayered Structures and Solid Solutions for Use in MIM Capacitors. *J. Electrochem. Soc.* **2005**, *152*, F54. [[CrossRef](#)]
119. Fairbrother, F. *The Chemistry of Niobium and Tantalum*; Elsevier Publishing Company: Amsterdam, The Netherlands, 1967; ISBN 978-0444402059.

120. Mozalev, A.; Sakairi, M.; Takahashi, H. Structure, Morphology, and Dielectric Properties of Nanocomposite Oxide Films Formed by Anodizing of Sputter-Deposited Ta-Al Bilayers. *J. Electrochem. Soc.* **2004**, *151*, F257. [[CrossRef](#)]
121. Zainulin, Y.G.; Alyamovskii, S.I.; Shveikin, G.P.; Popova, S.V. Possibility of Preparing Zirconium and Tantalum Monoxides at High Pressures and Temperatures. *Zh. Neorg. Khim.* **1978**, *23*, 1155–1157.
122. Lantelme, F.; Barhoun, A.; Li, G.; Besse, J. Electrodeposition of Tantalum in NaCl–KCl–K₂TaF₇ Melts. *J. Electrochem. Soc.* **1992**, *139*, 1249–1255. [[CrossRef](#)]
123. Chamelot, P.; Palau, P.; Massot, L.; Savall, A.; Taxil, P. Electrodeposition Processes of Tantalum(V) Species in Molten Fluorides Containing Oxide Ions. *Electrochim. Acta* **2002**, *47*, 3423–3429. [[CrossRef](#)]

Disclaimer/Publisher’s Note: The statements, opinions and data contained in all publications are solely those of the individual author(s) and contributor(s) and not of MDPI and/or the editor(s). MDPI and/or the editor(s) disclaim responsibility for any injury to people or property resulting from any ideas, methods, instructions or products referred to in the content.